Title

Repression by the *Arabidopsis* TOPLESS corepressor requires association with the core Mediator complex

Authors

Alexander R. Leydon[1], Wei Wang[2,†], Hardik P. Gala[1], Sabrina Gilmour[1], Samuel Juarez-Solis[1], Mollye L. Zahler[1], Joseph E. Zemke[1], Ning Zheng[2,3], Jennifer L. Nemhauser[1*]

[1]Department of Biology, University of Washington

[2]Department of Pharmacology & [3]Howard Hughes Medical Institute, University of Washington

[†]Present address: Key Laboratory of Plant Stress Biology, State Key Laboratory of Cotton Biology, School of Life Science, Jinming Campus, Henan University, Kaifeng, Henan Province, 475004, PR of China.

*Lead Contact.

Abstract

The plant corepressor TOPLESS (TPL) is recruited to a large number of loci that are selectively induced in response to developmental or environmental cues, yet the mechanisms by which it inhibits expression in the absence of these stimuli is poorly understood. Previously, we had used the N-terminus of *Arabidopsis thaliana* TPL to enable repression of a synthetic auxin response circuit in *Saccharomyces cerevisiae* (yeast). Here, we leveraged the yeast system to interrogate the relationship between TPL structure and function, specifically scanning for repression domains. We identified a potent repression domain in Helix 8 located within the CRA domain, which directly interacted with the Mediator middle domain subunits Med21 and Med10. Interactions between TPL and Mediator were required to fully repress transcription in both yeast and plants. In contrast, we found that multimer formation, a conserved feature of many corepressors, had minimal influence on the repression strength of TPL.

Keywords

Corepressors, Transcriptional Repression, Mediator, Tup1, TOPLESS

36 **Introduction**

37 Control over gene expression is essential for life. This is especially evident during development
38 when the switching of genes between active and repressed states drives fate determination.
39 Mutations that interfere with repression lead to or exacerbate numerous cancers (Wong et al.,
40 2014) and cause developmental defects in diverse organisms (Grbavec et al., 1998; Long et al.,
41 2006), yet many questions remain about how cells induce, maintain, and relieve transcriptional
42 repression. Transcriptional repression is controlled in part by a class of proteins known as
43 corepressors that interact with DNA-binding transcription factors and actively recruit repressive
44 machinery. Transcriptional corepressors are found in all eukaryotes and include the animal
45 SMRT (silencing mediator of retinoic acid and thyroid hormone receptor) and NCoR (nuclear
46 receptor corepressor) complexes (Mottis et al., 2013; Oberoi et al., 2011), the yeast Tup1
47 (Keleher et al., 1992; Matsumura et al., 2012; Tzamarias and Struhl, 1994), and its homologs
48 Drosophila Groucho (Gro) and mammalian transducing-like enhancer (TLE) (Agarwal et al.,
49 2015).

50 In plants, the role of Gro/TLE-type corepressors is played by TOPLESS (TPL),
51 TOPLESS-RELATED (TPR1-4), LEUNIG (LUG) and its homolog (LUH), and High Expression of
52 Osmotically responsive genes 15 (HOS15) (Causier et al., 2012; Lee and Golz, 2012; Liu and
53 Karmarkar, 2008; Long et al., 2006; Zhu et al., 2008). Plant corepressors share a general
54 structure, where at the N-terminus a LIS1 homology (LisH) domain contributes to protein
55 dimerization (Delto et al., 2015; Kim et al., 2004). At the C-terminus, WD40 repeats form beta-
56 propeller structures that are involved in protein-protein interactions (Collins et al., 2019; Liu et
57 al., 2019). In TPL family corepressors, the LisH is followed by a C-terminal to LisH (CTLH)
58 domain that binds transcriptional repressors through an Ethylene-responsive element binding
59 factor-associated Amphiphilic Repression (EAR) motif found in partner proteins (Causier et al.,
60 2012; Kagale et al., 2010). The N-terminal domain also contains a CT11-RanBPM (CRA)
61 domain, which provides a second TPL dimerization interface and stabilizes the LisH domain (Ke
62 et al., 2015; Martin-Arevalillo et al., 2017). The beta-propellers bind to the non-EAR TPL
63 recruitment motifs found in a subset of transcriptional regulators (RLFGV- and DLN-type motifs,
64 (Collins et al., 2019; Liu et al., 2019)), and may control protein interaction with other repressive
65 machinery. Defects in the TPL family have been linked to aberrant stem cell homeostasis
66 (Busch et al., 2010), organ development (Gonzalez et al., 2015), and hormone signaling

67 (Causier et al., 2012; Kagale et al., 2010), especially the plant hormone auxin (Long et al.,
68 2006).
69 We have previously demonstrated the recapitulation of the auxin response pathway in
70 *Saccharomyces cerevisiae* (yeast) by porting individual components of the *Arabidopsis* auxin
71 nuclear response (Pierre-Jerome et al., 2014). In this *Arabidopsis thaliana* Auxin Response
72 Circuit in *Saccharomyces cerevisiae* (*At*ARC^{Sc} - Figure 1A), an auxin responsive transcription
73 factor (ARF) binds to a promoter driving a fluorescent reporter. In the absence of auxin, the ARF
74 protein activity is repressed by interaction with a full-length Aux/IAA protein fused to the N-
75 terminal domain of TPL. Upon the addition of auxin, the TPL-IAA fusion protein is targeted for
76 degradation through interaction with a member of the Auxin Signaling F-box protein family, and
77 releases the transcriptional repression of the fluorescent reporter. Reporter activation can be
78 quantified after auxin addition by microscopy or flow cytometry (Pierre-Jerome et al., 2014). In
79 the original build and characterization of *At*ARC^{Sc}, it was noted that the two N-terminal
80 truncations of TPL (N100 or N300) behave differently (Pierre-Jerome et al., 2014). While both
81 truncations are able to repress the function of a transcriptional activator fused to an Aux/IAA,
82 only the TPLN100 fusion shows alleviation of repression after auxin addition. TPLN300 fusions
83 to Aux/IAAs maintain strong durable repression even under high concentrations of auxin. This
84 disparity is not due to differential rates of protein degradation, as both proteins appear to be
85 turned over with equal efficiency after auxin addition (Pierre-Jerome et al., 2014).
86 The conservation of TPL's repressive function in yeast suggests that the protein partners
87 that enact repression are conserved across eukaryotes. Consistent with this speculation, the
88 series of alpha-helices that form the N-terminal portion of TPL (Figure 1B) (Martin-Arevalillo et
89 al., 2017) is highly reminiscent of naturally-occurring truncated forms of mammalian TLE
90 (Gasperowicz and Otto, 2005), such as Amino-terminal Enhancer of Split (AES) (Zhang et al.,
91 2010), the Groucho ortholog LSY-22 (Flowers et al., 2010), and the unrelated mouse repressor
92 protein MXI1 (Schreiber-Agus et al., 1995). Gro/TLE family members are generally considered
93 to repress by recruiting histone deacetylases to control chromatin compaction and availability for
94 transcription (Chen and Courey, 2000; Long et al., 2006). An alternative hypothesis has been
95 described for Tup1 in yeast, where Tup1 blocks the recruitment of RNA Polymerase II (Pol-II)
96 (Wong and Struhl, 2011), possibly through contacts with Mediator complex subunits Med21 or
97 Med3 (Gromöller and Lehming, 2000; Papamichos-Chronakis et al., 2000). However, like many
98 of these family members, multiple repression mechanisms have been described for TPL at

99 different genetic loci. For example, TPL has been found to recruit the repressive CDK8 Mediator
100 complex (Ito et al., 2016), chromatin remodeling enzymes such as Histone Deacetylase 19
101 (HD19) (Long et al., 2006) and directly bind to histone proteins (Ma et al., 2017).
102 Here, we leveraged the power of yeast genetics to interrogate the mechanism of TPL
103 repression. Using *At*ARC^{Sc}, we discovered that the N-terminal domain of TPL contains two
104 distinct repression domains that can act independently. We mapped the first, weaker repression
105 domain to the first 18 amino acids of the LisH domain (Helix 1), and the second, more potent
106 domain to Helix 8 which falls within the CRA domain. Full repression by Helix 8 required the
107 Mediator complex, specifically direct interaction with Med21 and Med10. This interaction
108 required the same Med21 residues that control transcriptional activation of Tup1-regulated
109 genes in yeast. In addition, we found that multimerization of TPL was not required for repression
110 in yeast or in plants. Our yeast results were validated with plant assays, and extended to include
111 evidence that interaction with the middle domain of Mediator was required for TPL repression of
112 the auxin-regulated development program giving rise to lateral roots. Our findings point to a
113 conserved functional connection between Tup1/TPL corepressors and the Mediator complex
114 that together create a repressed state poised for rapid activation.
115
116 **Results**
117 To understand how TPL represses transcription, we first localized repressive activity within the
118 protein using the *At*ARC^{Sc} (Figure 1A). The extent of auxin-induced turnover of TPLN100 and
119 TPLN300 fusion proteins appears similar, although neither are completely degraded (Pierre-
120 Jerome et al., 2014). In this way, auxin sensitizes the *At*ARC^{Sc} to even subtle differences in the
121 strength of repressive activity by reducing the relative concentration of the TPL fusion proteins.
122 To pinpoint the region conferring the strong repression of TPL300, we generated a deletion
123 series of the N-terminus guided by the available structural information (Figure 1B-C, (Ke et al.,
124 2015; Martin-Arevalillo et al., 2017)).
125 We started by identifying a shorter truncation, TPLN188, which behaved identically to
126 TPLN300 (Figure 1D, (Pierre-Jerome et al., 2014)). Subsequently, we deleted each alpha
127 helical domain starting with Helix 9 (constructs are named in the format Helix x – Helix y or Hx-
128 Hy). We found that Helix 8 was required for the maximum level of repression activity and for the
129 maintenance of repression after auxin addition (Figure 1D). All constructs lacking Helix 8
130 retained the ability to repress transcription, but this repression was lifted in the presence of

131 auxin (Figure 1D) as had been observed for the original TPLN100 construct (Pierre-Jerome et
132 al., 2014). In addition to the repressive activity of Helix 8, further deletions revealed that the 18
133 amino acids of Helix 1 were sufficient to confer repression on their own (H1, Figure 1E). To test
134 whether Helix 8 activity depended on Helix 1, we analyzed a construct consisting of Helix 3
135 through Helix 9 (H3-H9, Figure 1D), which was able to repress transcription. Thus, Helix 1
136 (LisH) and Helix 8 (CRA) could contribute to TPL-mediated repression on their own (Figure 1D).
137 To identify the minimal domain required for Helix 8-based repression, we generated
138 additional deletions (Figure 1C,F, Figure 1 - Figure Supplement 1). Helix 8 and the following
139 linker were not sufficient for repression (Figure 1F), and removal of Helix 9 or of the linker
140 between Helix 8 and Helix 9 slightly increased sensitivity to auxin compared to TPLN188 (H1-
141 H8Δ8L, Figure 1 - Figure Supplement 1). A deletion that removed both the LisH and Helix 8
142 repression domains (H3-H7) was only able to weakly repress reporter expression (Figure 1 -
143 Figure Supplement 1). These results demonstrate that Helix 8, in combination with the linker
144 between Helix 8 and Helix 9 (which folds over Helix 1), was required for repression following
145 addition of auxin. Moreover, the repressive activity of Helix 8 and the linker were only functional
146 in the context of the larger Helix 3-Helix 8 truncation that carries the CTLH domain and a portion
147 of the CRA domain.
148

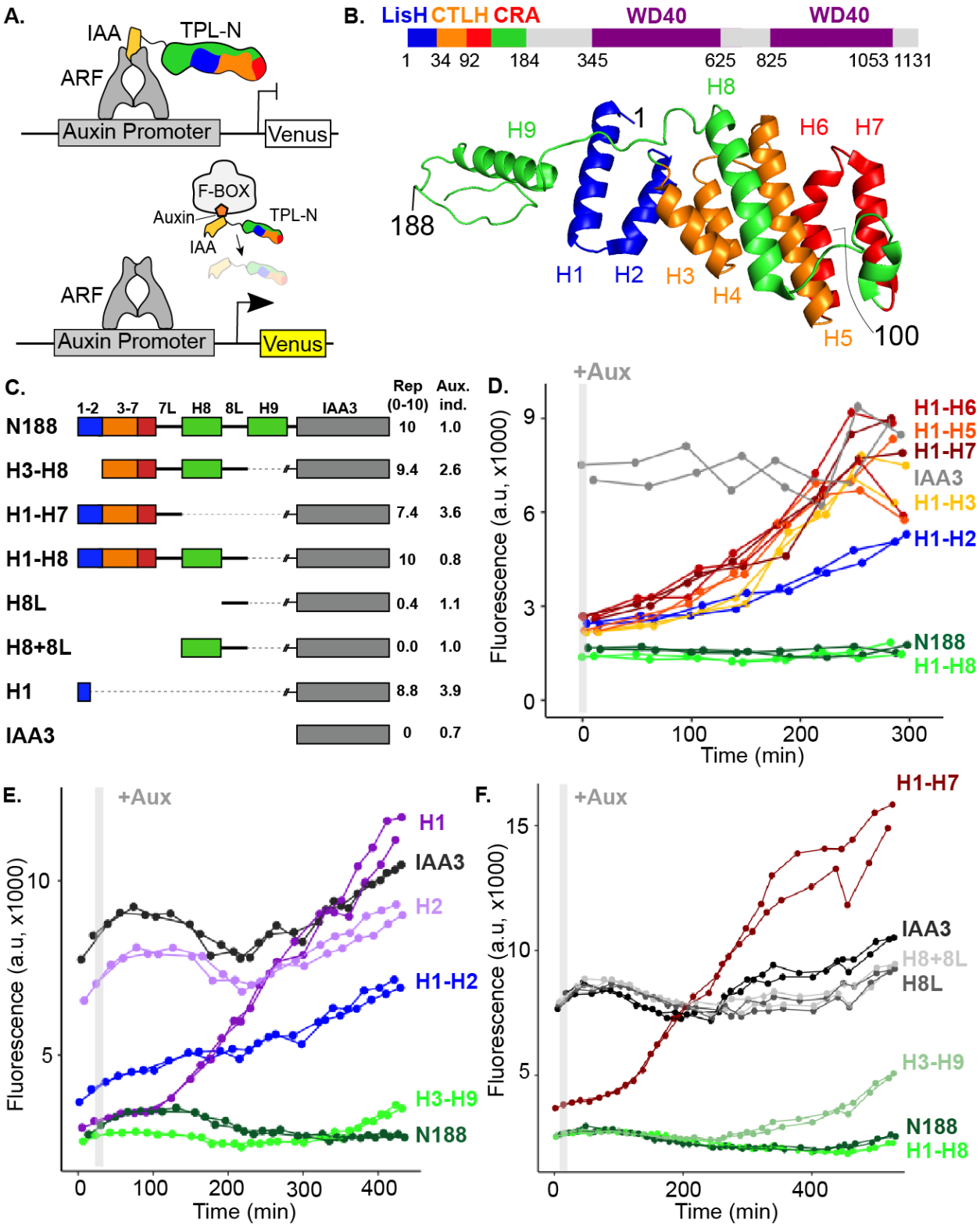

Figure 1. The N-terminal domain of TPL contains two independent repression domains.

A. Schematic of the ARC^{Sc}. The auxin responsive promoter driving the fluorescent protein Venus carries binding sites for the ARF transcription factor. In the absence of Auxin the IAA-

153 TPL fusion protein is bound to the ARF and maintains the circuit in a repressed state. Upon
154 addition of auxin the IAA-TPL protein is targeted for ubiquitination and subsequent protein
155 degradation, activating transcription of the fluorescent reporter. **B.** TPL domains are LisH (LIS1
156 homology motif, blue), CTLH (C-terminal LisH motif, orange), CRA (CT11-RanBPM, red -
157 dimerization and green - foldback), and two WD40, beta-propeller motifs (purple). N-terminal
158 domains are indicated on the solved structure of the first 202 amino acids ((Martin-Arevalillo et
159 al., 2017), 5NQS). The termini of the TPL-N100 truncation used in the original ARC^{Sc} studies is
160 indicated. **C.** Diagram indicating the structure of constructs analyzed in experiments shown in
161 subsequent panels. Repression Index (Rep.) is a scaled measure of repression strength with 0
162 set to the level of repression observed with IAA3 and 10 set to the level of repression by
163 TPLN188-IAA3. Auxin induction level (Aux. ind.) indicates the fold change difference between
164 reporter expression before auxin addition (time zero) and at the end of an experiment (~500
165 minutes) **D-F.** Helix 1 and the CRA domain (Helix 3-Helix 8) can act independently to repress
166 transcription. Each panel represents two independent time course flow cytometry experiments
167 of the TPL helices indicated, all fused to IAA3. Every point represents the average fluorescence
168 of 5-10,000 individually measured yeast cells (a.u. - arbitrary units). Auxin (IAA-10μM) was
169 added at the indicated time (gray bar, + Aux).
170
171 To determine which of the many known or predicted TPL-binding partners could mediate
172 the repression activity of Helix8, we identified known interactors with either TPL or other
173 Gro/TLE co-repressors, and then introduced the *Arabidopsis* homologs of these genes into the
174 cytoplasmic split-ubiquitin (cytoSUS) system (Asseck and Grefen, 2018). We chose the
175 cytoSUS system over yeast two-hybrid, because in cytoSUS the interaction between target
176 proteins takes place in the cytoplasm, and we had observed that the TPL N-terminus could
177 repress activation of yeast two hybrid prototrophy reporters (Figure 1D, Figure 2 – Figure
178 Supplement 1A). Putative direct interactors include histone deacetylases (HDACs - AtHDAC9,
179 AtHDAC6, (Long et al., 2006)), Histone proteins (Histone H3, Histone H4, (Ma et al., 2017)),
180 and the Mediator components MED13 (AtMED13, (Ito et al., 2016)) and MED21, which has
181 been demonstrated to interact with Tup1, the yeast homolog of TPL (Gromöller and Lehming,
182 2000). We did not observe any interactions between TPL-N188 and the HDACs HDA6 and
183 HDA9; the histone protein AtHIS4; or the Mediator subunit AtMED13 (Figure 2A, Figure 2 –
184 Figure Supplement 1B). HDAC interaction with TPL has been previously hypothesized to occur
185 through indirect interactions with partner proteins (Krogan et al., 2012), however direct

186 interactions with histones and MED13 have been detected (Ito et al., 2016; Ma et al., 2017). The
187 absence of interaction between TPL-N188 and these proteins may be due to differences
188 between methods, or interaction interfaces in the C-terminal WD40 repeats.
189 Strong interaction was detected between TPL-N188 and AtMED21, a component of the
190 Mediator middle domain (Figure 2A). MED21 is one of the most highly conserved Mediator
191 subunits (Bourbon, 2008), and has a particularly highly conserved N-terminus (Figure 2 – Figure
192 Supplement 2A,C-E). In yeast, Tup1 interacts with the first 31 amino acids of ScMed21, with the
193 first seven amino acids being absolutely required (Gromöller and Lehming, 2000). We observed
194 that the equivalent truncation of AtMED21 (AtMED21-N31) was sufficient for interaction with
195 TPL-N188 (Figure 2A). We next created truncations of the N-terminal domain of AtMED21 to
196 closely match those that had been made in yeast (Figure 2B, Figure 2 – Figure Supplement 1B)
197 where deletion of the first five amino acids of ScMed21 (ScΔ5Med21) severely reduce the ability
198 of the Mediator complex to co-purify with Pol-II and CDK8 kinase complex (Sato et al., 2016).
199 Interaction between TPLN188 and AtMED21 similarly required the first five amino acids of
200 AtMED21 (Figure 2B), and, as in yeast, this was not a result of destabilization of the AtMED21
201 protein (Figure 2B). AtMED21 interaction was specific to the Helix8-based repression domain,
202 as it interacted with TPLH3-H9 (Figure 2E), and not TPLH1-H5 (Figure 2 – Figure Supplement
203 1C). Further screening of middle domain Mediator components identified an additional
204 interaction with AtMED10B, the predominantly expressed MED10 isoform in *Arabidopsis*
205 (Klepikova et al., 2016) (Figure 2C). Interactions between TPLN188 and both AtMED21 and
206 AtMED10B were confirmed by immunoprecipitation (Figure 2D).
207

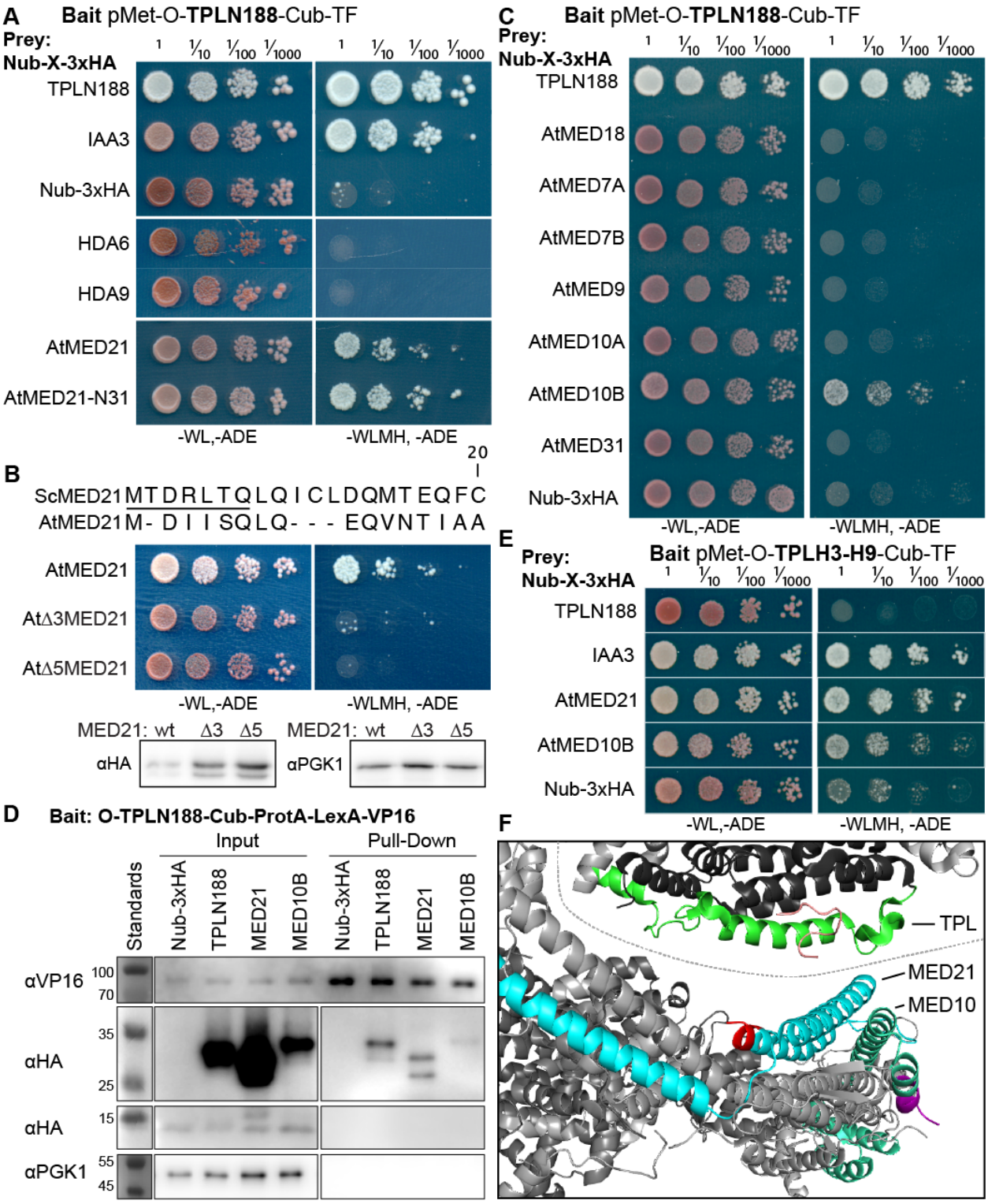

Figure 2. The Helix 8 repression domain of TPL directly interacts with AtMED21 and AtMED10B. A-C,E. cytoSUS assays with candidate interacting proteins. Nub-3xHA is the N-terminal fragment of Ubiquitin expressed with no fusion protein and is used as a negative control. Each prey protein is from *Arabidopsis*. -WL, -ADE - dropout lacking Trp, Leu and Ade

213 (growth control), -WLMH, -ADE – dropout lacking Trp, Leu, His, Met, and Ade (selective media).
214 The plating for each panel was performed at the same day, white lines are provided when plates
215 were cropped for clarity. **B**. Alignments of the *Arabidopsis* (At) and *Saccharomyces* (Sc) MED21
216 proteins are shown above cytoSUS assays with the same bait shown in (**A)**. Western blots
217 below the colonies indicated that AtMED21 N-terminal Δ3 and Δ5 are well expressed in assay
218 conditions. **C.** cytoSUS assays with selected Mediator proteins in the middle module. **D.** The
219 TPL-ProteinA-TF fusion protein can pull down TPL, AtMED21 and AtMED10B from yeast
220 extracts using IgG-beads. Detection of the VP16 transcriptional activator demonstrates
221 enrichment of the fusion protein (αVP16). Each prey protein is detected via the 3xHA tag (αHA),
222 and efficacy of purification was judged by PGK1 depletion (αPGK1). **E.** A TPL-N truncation
223 lacking the LisH domain (TPLH2-H9) could still interact with the AtMED21-N31 truncation. This
224 bait construct interacted with IAA3, but only minimally with the negative control (free Nub-3xHA).
225 **F.** Yeast Mediator (bottom, 5N9J) and AtTPL (top, 5NQV) manually juxtaposed to compare
226 relative domain sizes and feasibility of a TPL-MED21-MED10B interaction. TPL Helix 8-9 is
227 colored green. MED21 is colored aqua, with the N-terminus colored red, and the EAR peptide in
228 orange. MED10 is colored teal, with the C-terminus colored purple. The dotted line indicates the
229 border between TPL and Mediator structures.
230
231 A manual juxtaposition of the yeast Mediator structure with the *Arabidopsis* TPL N-
232 terminal structure shows that Helix 8 and the linker following face away from the tetramer and
233 are therefore optimally placed to interact with Mediator components (Figure 2F). To pinpoint
234 which residues of Helix 8 coordinate repression through interaction with MED21, we identified
235 solution-facing amino acids (Martin-Arevalillo et al., 2017) (Figure 1C). We reasoned that such
236 residues were most likely not involved in stabilizing the hydrophobic interactions between intra-
237 TPL helical domains and could therefore be available to interact with partner proteins. Eight
238 amino acids in Helix 8 were mutated to alanine in the context of the H3-H8-IAA3 fusion protein
239 (Figure 3A, light green residues) to enable assessment of repression activity in the absence
240 (Figure 3B) or presence (Figure 3C) of auxin. No single amino acid was essential for repression.
241 Two mutations (R140A and K148A) slightly increased baseline expression of the reporter
242 (Figure 3B-C). With the exception of E152A, which behaved similarly to controls, all of the
243 mutations altered the stability of repression after auxin addition, either by increasing (S138A,
244 V145A, E146A, K149A) or decreasing (I142A) the final fluorescence level (Figure 3C). Mutating
245 E146 and K149 also increased the speed with which the reporter responded to auxin (Figure

246 3C), suggesting that these two neighboring residues could be a critical point of contact with co-
247 repressive machinery. S138A had a small increase in auxin sensitivity, while I142 reduced auxin
248 sensitivity (Figure 3E).
249 We next tested whether the residues in Helix 8 that were required for repression (V145,
250 E146, K148, K149, Figure 3A-C) were also required for interaction with AtMED21. Single
251 alanine mutations of these four amino acids in the context of TPLN188 significantly reduced
252 interaction with AtMED21, while the quadruple mutation (here called $Quad^{AAAA}$) completely
253 abrogated AtMED21 binding (Figure 3D). These mutations had little effect on interaction with
254 AtMED10B (Figure 2 – Figure Supplement 2D). Introduction of $Quad^{AAAA}$ mutations into the
255 Helix 3 through Helix 8 context (H3-H8-$Quad^{AAAA}$) in the *At*ARC^{Sc} largely phenocopied a deletion
256 of Helix 8 (yellow and pink, Figure 4E, compare to H3-H7, Figure 1 – Figure Supplement 1). In
257 contrast, TPLN188-$Quad^{AAAA}$ largely retained the repressive activity of wild-type N188 (red and
258 black, Figure 3E), consistent with the observation that Helix 1 is sufficient for full repression
259 (Figure 1D). These results indicate that the CRA domain (H3-H8) requires contact with MED21
260 to repress, and that this is independent of repression via Helix 1.
261

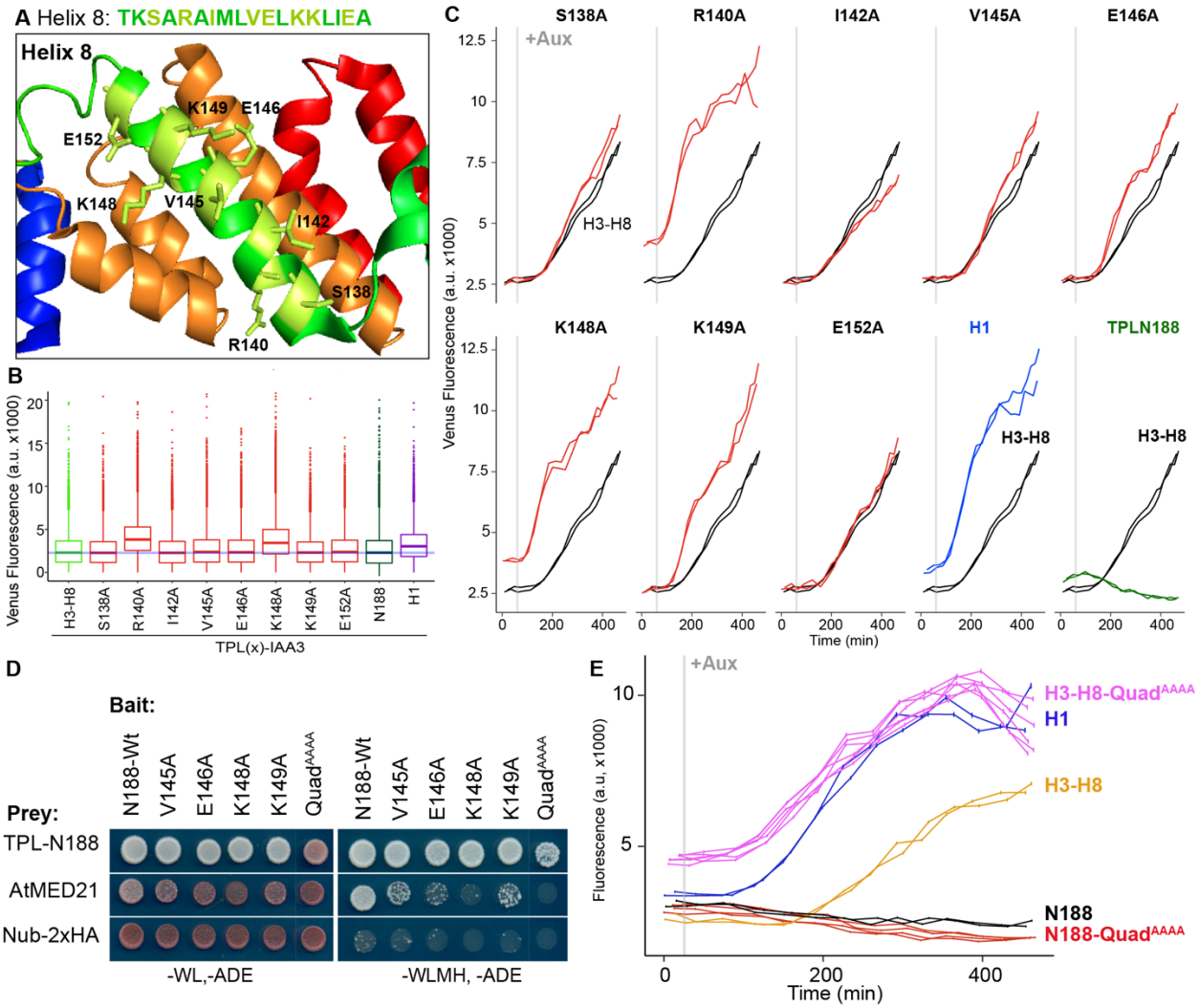

Figure 3. Identification of critical residues within Helix 8 repression domain. A. Sequence and structure of Helix 8 (5NQS). Helix 8 is colored green, and amino acids chosen for mutation are highlighted in light green in both the sequence and the structure. **B.** Repression activity of indicated single and double alanine mutations. **C.** Time course flow cytometry of selected mutations of Helix 8 following auxin addition. TPLH3-8-IAA3 fusion proteins (black) were compared to indicated single mutations to alanine (red). Controls - Helix 1 (H1 – blue), and TPLN188 (dark green). **D.** A series of alanine mutations (V145A, E146A, K148A, K149A, and the quadruple mutant Quad^{AAAA} chosen from Figure 2D-F) were introduced into the TPL-N188 bait construct and tested for interaction with wild-type TPL-N188, AtMED21 and controls. Each single alanine mutation reduces TPL interaction with AtMED21, while the quad mutation abrogated interaction. **E.** The Helix 8 Quad^{AAAA} mutation was introduced into the TPLN188-IAA3 and TPLH3-8-IAA3 fusion proteins and compared to wild type N188 in time course flow cytometry. For all cytometry experiments, the indicated TPL construct is fused to IAA3. Every

276 point represents the average fluorescence of 5-10,000 individually measured yeast cells (a.u. -
277 arbitrary units). Auxin (IAA-10μM) was added at the indicated time (gray bar, + Aux). At least
278 two independent experiments are shown for each construct.
279
280 The large Mediator complex stabilizes the pre-initiation complex (PIC) enabling
281 transcriptional activation (Kornberg, 2005; Nozawa et al., 2017; Roeder, 1996; Schilbach et al.,
282 2017). The connection we found between TPL, two Mediator components and transcriptional
283 repression raised the possibility that other parts of the Mediator complex might also contribute to
284 corepressor function. To test this, we needed a way to measure whether loss of function of
285 individual Mediator components led to de-repression at an individual locus. In the case of the
286 yeast corepressor Tup1, a standard approach has been to test the level of transcription at target
287 genes in the presence of deletion mutations of Tup1-interacting proteins (Gromöller and
288 Lehming, 2000; Lee et al., 2000; Zhang and Reese, 2004). One challenge to such an approach
289 for Mediator components is that loss of function mutants can be lethal or exhibit drastic
290 physiological phenotypes (Biddick and Young, 2005).
291 To avoid these complications, we turned to the well-established Anchor Away system for
292 inducible protein depletion (Haruki et al., 2008) and combined it with quantification of
293 transcriptional activity at the synthetic locus in the *At*ARC^{S} (Figure 4B). However, *At*ARC^{Sc}
294 integrates components at four genomic locations using prototrophic markers that are not
295 compatible with those needed for Anchor Away. To overcome this limitation, we re-recreated the
296 ARC on a single plasmid (we refer to this plasmid as SPARC) using the Versatile Genetic
297 Assembly System (VEGAS, (Mitchell et al., 2015)). SPARC behaved with similar dynamics to
298 the original *At*ARC^{Sc} on both solid and liquid growth conditions (Figure 4 – Figure Supplement
299 1A-C). As a first test of the Anchor Away system with SPARC, we fused Tup1 and its partner
300 protein Cyc8 to two copies of the FKBP12-rapamycin-binding (FRB) domain of human mTOR
301 (Haruki et al., 2008). Rapamycin treatment of strains targeting either of these proteins caused
302 no release of repression on the SPARC reporter, providing confirmation of orthogonality of the
303 synthetic system in yeast (Figure 4 – Figure Supplement 1D).
304 Before testing repressive function, we first performed chromatin immunoprecipitation
305 using the Anchor Away FRB tag to ask whether Mediator proteins or specific Mediator modules
306 were detectable at the promoters of TPL-repressed genes. We began by assaying the
307 integrated AtARC^{Sc} locus and comparing it to a Tup1-repressed locus, SUC2 (Carlson and

308 Botstein, 1982; Fleming and Pennings, 2007, p. 2; Trumbly, 1992). We generated a yeast strain
309 with an integrated MED21-FRB fusion protein and an integrated AtARC^{Sc} locus with a 2xHA
310 epitope-tagged TPLN188-IAA3 repressor protein. We observed enrichment of both MED21-FRB
311 and the 2xHA-TPLN188-IAA3 fusion protein at the AtARC^{Sc} locus (Figure 4C). We also
312 observed a modest enrichment (2-fold) of MED21-FRB at the SUC2 locus. Next, we introduced
313 the fully repressed SPARC plasmid containing TPLN188 (SPARC^{N188}) into a library of Anchor
314 Away yeast strains that allow specific depletion of Mediator components (see Figure 4A-B)
315 (Haruki et al., 2008; Petrenko et al., 2017). We tested representatives of the mediator complex
316 (Tail – Med15, Head – Med18, Middle – Med21 & Med14, Kinase – CDK8, Basal Transcription
317 Factors – TBP1, TFIIA, and RNA polymerase II – Rbp1) by ChIP-qPCR. We observed
318 enrichment of all tested core Mediator complex members, as well as Basal Transcription
319 Factors, at both the SPARC and the SUC2 loci, with very little enrichment of RNA polymerase II
320 (Figure 4D). Higher enrichment of members of the middle module (i.e. Med21, Med14, Figure
321 4D) may point to nucleation of the complex by assembly of the middle domain.
322 We next tested whether the association of Mediator complex components were required
323 for TPL-mediated repression (Figure 4A-B). Nuclear depletion of Mediator components from the
324 Tail, Head, and Middle domain triggered clear activation of the SPARC^{N188} reporter (Figure 4E-
325 I). Depletion of the Mediator kinase module component CDK8 had a more modest effect (Figure
326 4H). One caveat to this approach is that nuclear depletion of components that are absolutely
327 required for transcriptional activation, such as the Tail triple Anchor Away (17,3,15 - Figure 4E)
328 or the RNA Polymerase II (Pol II) Anchor Away (Rpb1 – Figure 4I), cannot be assayed for
329 impacts on repression using transcription of the reporter as the output.
330 To further interrogate the impact of Mediator on repression, we next focused on the
331 other side of the interaction, namely which region of MED21 was required for interaction with
332 TPL. Deletion of the first 7 amino acids of ScMed21 (Δ7Med21) partially activates genes that
333 are normally repressed by Tup1 (Gromöller and Lehming, 2000), so we first tested if the same
334 held true for TPL-mediated repression. We introduced SPARCs with different TPL constructs
335 into strains where wild-type ScMed21 or N-terminal deletions were targets of Anchor Away.
336 Importantly, the addition of the FRB tag did not alter ScMED21 function (Figure 4J, Figure 4 –
337 Figure Supplement 3E-F). We observed that deletion of either five or seven of the N-terminal
338 residues of ScMed21 increased the expression of the reporter in SPARC^{N188} to a level similar as
339 what is observed with TPL H1-H5 (Figure 4J, Figure 4 – Figure Supplement 1E-F). No mutation

340 increased the SPARC's sensitivity to auxin. As Δ7ScMed21 had a noticeable impact on growth,
341 as has been reported previously (Gromöller and Lehming, 2000; Hallberg et al., 2006), we
342 removed it from further studies. Δ5ScMed21 had no observable growth defects, although this
343 deletion is known to be sufficient to alter Mediator assembly and disrupt binding of Pol II and the
344 CDK8 kinase module (Hallberg et al., 2006; Sato et al., 2016).

345 The fully repressed SPARC^{N188} in Δ3ScMed21 or Δ5ScMed21 mutants showed elevated
346 reporter transcription when compared to strains carrying wild-type ScMED21 (Figure 4K). The
347 addition of Rapamycin further increased reporter expression, particularly in the Δ3ScMed21
348 strains, suggesting that this deletion could only partially disrupt the TPLN188-Med21 interaction.
349 We used chromatin immunoprecipitation to directly test whether Δ5Med21 showed a change in
350 association with the SPARC^{N188} promoter. While this deletion would be expected to reduce
351 association with TPL, the resulting de-repression of the locus should lead to an increase in
352 association with the activated promoter. Indeed, we observed a 1.6x fold increase in Δ5Med21-
353 FRB promoter binding compared to wild-type (Figure 4L). While this enrichment is modest
354 compared to a repressor-free SPARC^{IAA14} (Figure 4L, gray bar), it is correlated with the
355 magnitude of the increase in transcriptional activation of the reporter in the Δ5Med21 genotype
356 (Figure 4J-K). To confirm that the interaction with TPL was not unique to ScMed21, we replaced
357 the first five amino acids of ScMed21-FRB with the corresponding sequence from AtMED21.
358 The strain carrying this chimeric protein had an identical repression profile as the one with
359 native ScMed21 (Figure 4 – Figure Supplement 2B), and showed no difference in growth or
360 viability (Figure 4 – Figure Supplement 2C).

361 To minimize any possible off-target impact of ScMed21 deletions, we introduced
362 estradiol inducible versions of ScMed21 (iScMed21) into the Anchor Away SPARC^{N188} strains
363 (Figure 4 – Figure Supplement 4, (McIsaac et al., 2013)). The combination of all three synthetic
364 systems--ARC^{Sc}, Anchor Away and estradiol inducibility--made it possible to rapidly deplete the
365 wild type ScMed21-FRB from the nucleus while simultaneously inducing ScMed21 variants and
366 visualizing the impact on a single auxin-regulated locus. Depletion of nuclear ScMed21 by
367 Rapamycin increased levels of the reporter in all genotypes examined (Figure 4G,K) while
368 increasing cell size even in short time-courses, consistent with its essential role in many core
369 pathways (Figure 4 – Figure Supplement 3A, (Gromöller and Lehming, 2000)). When wild-type
370 iScMed21 was induced, there was a rescue of both reporter repression and cell size (Figure 4 –
371 Figure Supplement 4C,D), whereas induction of either Δ3 and Δ5 variants resulted in

372 significantly less reporter repression (Figure 4 – Figure Supplement 4D). iΔ3Med21 was
373 induced and accumulated at a comparable level to wild type Med21, while iΔ5Med21 is less
374 stable (Figure 4 – Figure Supplement 4E-F). In the time courses with both Rapamycin and
375 estradiol, we did not observe the cell size increases observed in the Rapamycin treatments
376 alone (populations were evenly distributed around a single mean), suggesting we were
377 observing the immediate effects of the Med21 deletions (Figure 4 – Figure Supplement 4G-H).

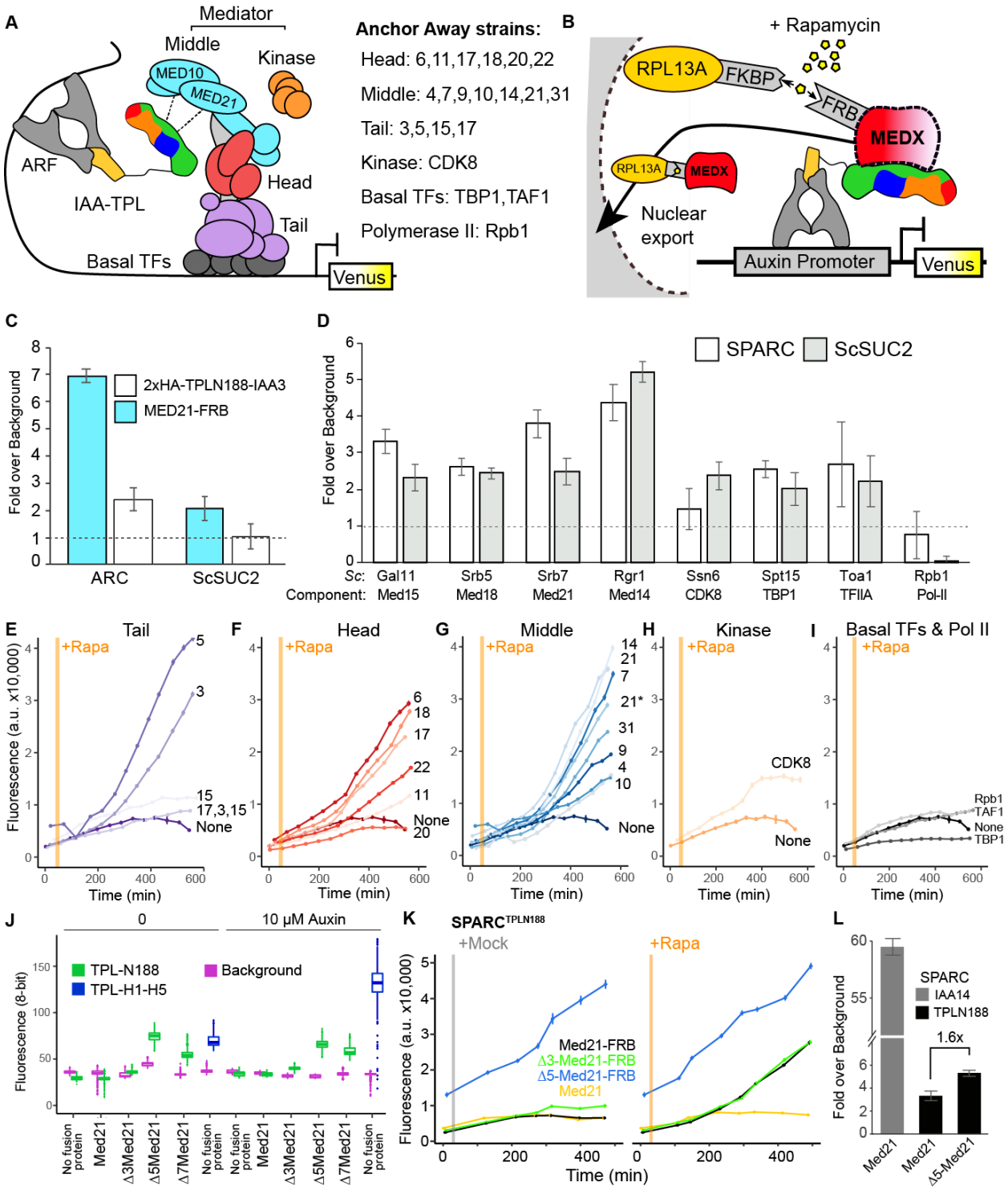

Figure 4. Repression by TPL requires interaction with the N-terminus of MED21 at promoters. A. Model of the proposed interaction between the TPL N-terminus with Mediator, where TPL interaction with Mediator 21 and 10 inhibit the recruitment of Pol-II. Proteins in this complex that were tested by Anchor Away are listed on the right. **B.** Schematic of *At*ARC^{Sc} combined with methods for inducible expression and nuclear depletion of MED21. In Anchor

384 Away, the yeast ribosomal protein 13A (RPL13A) is fused to the rapamycin binding protein
385 FKBP. Addition of Rapamycin induces dimerization between FKBP and any target protein fused
386 to 2xFRB, resulting in removal of the target protein from the nucleus. For these experiments,
387 *At*ARC^{Sc} was assembled into a single plasmid (SPARC) rather than being integrated into
388 separate genomic loci (Figure 4 – Figure Supplement 1). **C.** 2xHA-TPLN188-IAA3 and MED21-
389 FRB association with the ARC and the ScSUC2 promoters. ChIP was performed with αHA and
390 αFRB before qPCR was used to quantify enrichment at specified loci. **D.** Association of FRB-
391 tagged components of Mediator and the transcriptional machinery with the SPARC plasmid and
392 the ScSUC2 promoters. ChIP was performed with αFRB and qPCR was used to quantify
393 enrichment at specified loci. **E-I.** Time-course flow cytometry analysis of SPARC^{N188} in Mediator
394 Anchor Away yeast strains with Rapamycin (orange bar, + Rapa). Two Med21 strains were
395 compared in the Middle domain (E), 21 (generated in this study) and 21* (generated in
396 (Petrenko et al., 2017)). Both 21 and 21* demonstrated similar increases in reporter expression.
397 **J.** Quantification of Venus fluorescence from SPARC^{N188} in wild type and N-terminal ScMed21
398 deletions with and without auxin. The x-axis indicates strain and which FRB fusion protein is
399 being tested. Yeast was grown for 48 hours on SDO media with or without auxin and colony
400 fluorescence was quantified and plotted with the auxin responsive SPARC^{H1-H5} in wild type as a
401 reference. Background - red autofluorescence was used as a reference for total cell density. **K.**
402 Time-course flow cytometry analysis of SPARC^{N188} in wild type and N-terminal ScMed21
403 deletions with and without Rapamycin. Genotypes are indicated in the colored key inset into the
404 graph. For (**E-I, K**) a.u. - arbitrary units. Rapamycin was added at the indicated time (orange
405 bar, + Rapa). Every point represents the average fluorescence of 5-10,000 individually
406 measured yeast cells. **L.** Association of MED21-FRB or Δ5-MED21-FRB with SPARC plasmids.
407 ChIP was performed with αFRB and qPCR was used to quantify enrichment at specified loci. **C-**
408 **D,L.** A region of the ACT1 gene body was arbitrarily defined as background, and data is
409 presented as fold enrichment over the control gene. Averages and standard errors of four
410 replicates are shown.
411
412 Several lines of evidence suggest that, in addition to interactions with other partners,
413 homomultimerization modulates TPL repression potential. First, structures of the N-terminal
414 domains of TPL (Martin-Arevalillo et al., 2017) and a rice homolog OsTPR2 (Ke et al., 2015)
415 reveal high conservation of residues that coordinate formation of homotetramers and connect
416 tetramer formation to Aux/IAA binding. Second, the dominant TPL mutant *tpl-1* altered a single

417 amino acid in the ninth helix of the TPL-N terminus (N176H) that induces aggregation of TPL
418 and its homologs (TPR1-4), reducing total activity (Long et al., 2006; Ma et al., 2017). Third,
419 TPL recruitment motifs found in the rice strigolactone signaling repressor D53 induce higher-
420 order oligomerization of the TPL N-terminus, which increases histone binding and transcriptional
421 repression (Ma et al., 2017). Our studies in yeast suggest there may be a more complex
422 relationship between tetramer formation and repression, as we have measured strong
423 repressive activity in several constructs that are unlikely (TPLN100 (Pierre-Jerome et al., 2014))
424 or unable (H1, H3-8; Figure 1C) to form tetramers (compare Figure 1B with Figure 5A). To
425 quantify the potential for interaction among our constructs, we used the cytoSUS assay (Asseck
426 and Grefen, 2018). Helix 8 was required for strongest interaction between TPL constructs
427 (Figure 5 – Figure Supplement 1A), although this assessment was complicated by the fact that
428 some of the shorter constructs accumulated to significantly lower levels (Figure 5 – Figure
429 Supplement 1B). The weak interaction we could observe between full-length TPL-N and the
430 Helix 1 through Helix 3 construct (H1-3), indicated that the TPL LisH domain is sufficient for
431 dimerization. Therefore, while auxin-insensitive repression may require multimeric TPL, this
432 higher-order complex was not required for auxin-sensitive repression mediated by Helix 1
433 (Figure 1E).
434 To avoid any potential artifacts from analysis of truncated forms of the N-terminus, we
435 next generated site-specific mutations that disrupted multimerization in the context of TPLN188.
436 Martin-Arevalillo et al. had previously identified a triple mutation (K102S-T116A-Q117S-E122S)
437 that abrogated the ability of the CRA domain (Helix 6 and Helix 7) to form inter-TPL interactions
438 (Martin-Arevalillo et al., 2017). As this mutant form of TPL is only capable of dimerizing through
439 its LisH domain, we refer to it here as LDimer (Figure 5A). The LDimer mutations in TPLN188
440 retained the same auxin insensitive repression auxin behavior as wild-type TPLN188 (Figure
441 5D), supporting the finding from the deletion series.
442 To make a fully monomeric form of TPL, we introduced mutations into the dimerization
443 interface of the LisH domain in the context of LDimer. We first mutated one of a pair of
444 interacting residues (F15) to a series of amino acids (Tyrosine - Y, Alanine - A, Arginine - R, or
445 Aspartic Acid - D) in the context of either LDimer (Figure 5D), or H1-2 (Figure 5B, 5E).
446 Conversion of F15 to the polar and charged aspartic acid (D) completely abolished repression
447 activity, while the positively charged arginine was better tolerated (Figure 5D,E). The conversion
448 of F15 to tyrosine had no effect on LDimer (Figure 5D), and only a minimal increase in auxin

449 sensitivity in the context of H1-2 (Figure 5E). We then combined LDimer-F15Y with a mutation
450 of the coordinating residue L8 to serine with the intention of stabilizing the now solvent-facing
451 residues. The repressive behavior of this mutant was indistinguishable from that of LDimer
452 (Figure 5F).
453 To further push the LDimer towards a monomeric form, we introduced two additional
454 mutations (S5A, E19S, Figure 5C,G). Size exclusion chromatography confirmed that this
455 combination of mutations (S5A-L8S-F15Y-E19S-K102S-T116A-Q117S-E122S, hereafter called
456 Monomer) successfully shifted the majority of the protein into a monomeric state (Figure 5H);
457 however, this shift had no observable impact on repression strength before or after auxin
458 addition (Figure 5G). To test whether these mutations had a similar impact on *in vivo* TPL
459 complexes, we introduced the LDimer and Monomer mutations into the cytoSUS assay. In
460 contrast to the *in vitro* chromatography results with purified proteins, Monomer expressed in
461 yeast retained measurable interaction with wild-type TPL, LDimer or Monomer, albeit at a
462 reduced level than what was observed between wild type TPLN188 constructs (Figure 5I). A
463 caveat to this apparent difference between assays is that the Monomer mutations led to a
464 striking increase in protein concentration in yeast (Figure 5 – Figure Supplement 1C), likely
465 partially compensating for the decrease in affinity.
466

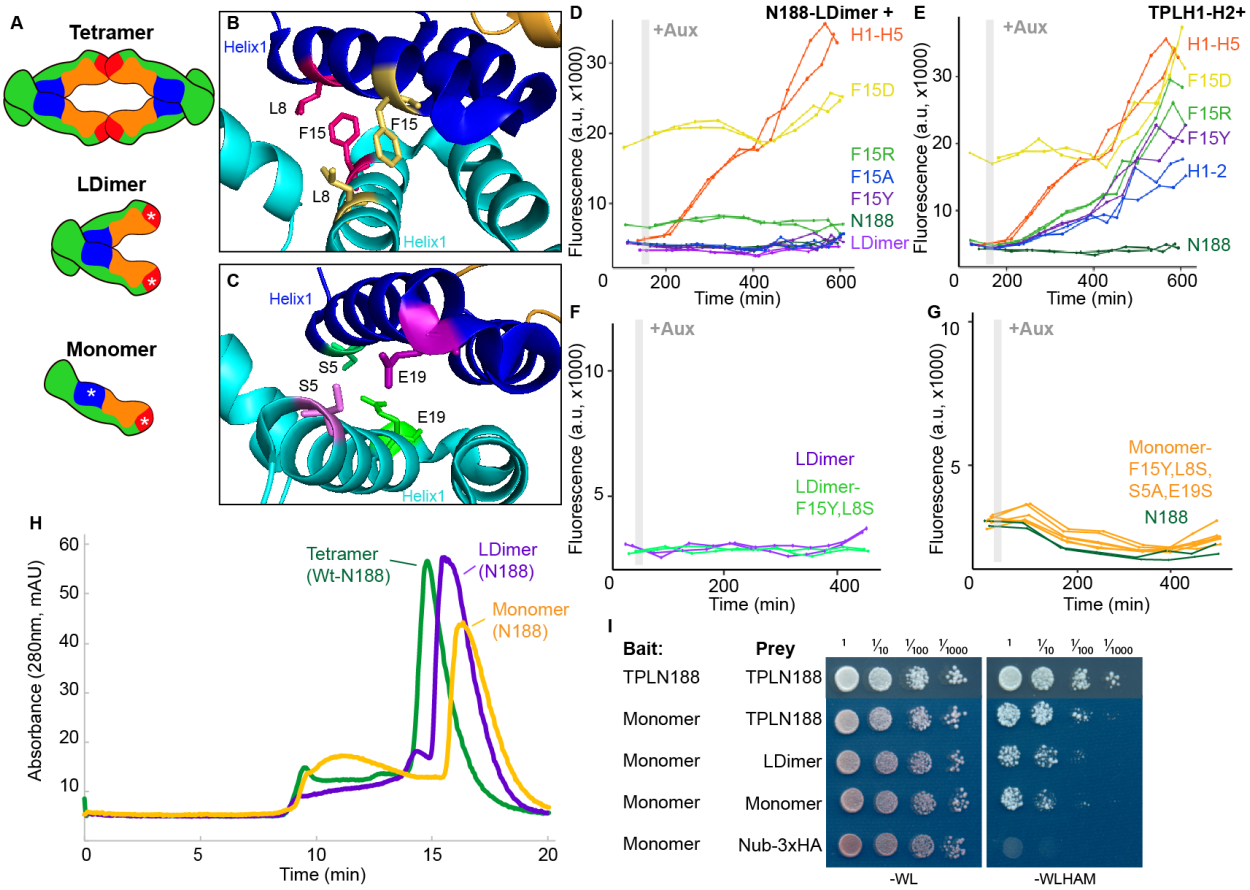

Figure 5. Multimerization is not required for repression in yeast. A. TPL can form a homotetramer via the CRA (red) and LisH (blue) domains. Asterisks indicate mutations that block or diminish these interactions. **B-C**. Locations of critical positions in Helix 1 are highlighted for two interacting TPL monomers (shown in light and dark blue). Interacting amino acids share the same color (adapted from 5NQV). **D-G.** Time course flow cytometry analysis of TPLN-IAA3 fusion proteins carrying selected single point mutations in N188-LDimer-IAA3 (**D**) and the TPLH1-2 truncation (**E**). The F15Y mutation had little effect on repression activity for either TPL construct. Double mutations (F15Y, L8S in LDimer) (**F**) or the quadruple Monomer mutations (S5A, L8S, F15Y, E19S in LDimer) (**G**) showed repression activity that was indistinguishable from LDimer or wild type N188 fused to IAA3. For all cytometry experiments, the indicated TPL construct is fused to IAA3. Every point represents the average fluorescence of 5-10,000 individually measured yeast cells (a.u. - arbitrary units). Auxin (IAA-10μM) was added at the indicated time (gray bar, + Aux). At least two independent experiments are shown for each construct. **H**. Size Exclusion Chromatography on TPLN188 wild type (green), LDimer (purple) and Monomer (orange) tetramerization mutants. **I**. CytoSUS on TPL tetramerization mutants.

485 To ascertain which of our findings about TPL required the sensitivity and simplicity of the
486 synthetic context and which could be observed in the full complexity of intact plant systems, we
487 performed a set of experiments in *Nicotiana benthamiana* (tobacco) and *Arabidopsis.*
488 Bimolecular Fluorescence Complementation (BiFC) confirmed the interaction between TPL and
489 MED21 (Figure 6A), which was further validated by co-immunoprecipitation using tobacco
490 extracts (Figure 6B). We were also able to pull down MED21 and TPL using MED10B (Figure 6
491 – Figure Supplement 1A). BiFC also confirmed the importance of the same TPL Helix 8
492 residues for the TPL-AtMed21 interaction (Figure 6A, $TPL^{H8QuadA}$). Similarly, the Δ5AtMED21 N-
493 terminal truncation eliminated interaction with full-length TPL (Figure 6A). We next developed a
494 quantitative repression assay based on UAS/GAL4-VP16 (Brand and Perrimon, 1993) (Figure
495 6C). To block potentially confounding interactions with endogenous TPL/TPRs or TIR1/AFBs,
496 we engineered a variant of IAA14 with mutations in the two EAR domains (EAR^{AAA}) and in the
497 degron (P306S) ($IAA14^{mED}$; Figure 6C). After prototyping the system in yeast (Figure 6 – Figure
498 Supplement 1B-C), we quantified repression strength of constructs carrying *TPLN-IAA14*^{mED}
499 variants using the well-characterized synthetic auxin responsive promoter DR5 (Ulmasov et al.,
500 1997). As expected, DR5 was strongly induced by co-transformation with AtARF19, and this
501 induction was sharply reduced by the inclusion of *UAS-TPLN188-IAA14*^{mED} and *GAL4-VP16*
502 (Figure 6 – Figure Supplement 1D). Overall, we observed strong correlation in repression
503 activity between what was observed in yeast and in tobacco.
504 To connect the observed differences in repression strength to a developmental context,
505 we generated transgenic *Arabidopsis* lines where the UAS-TPL-$IAA14^{mED}$ constructs were
506 activated in the cells where IAA14 normally acts to regulate the initiation of lateral root primordia
507 (Figure 6D, (Gala et al., 2020; Laplaze et al., 2005)). Expression of functional TPL-$IAA14^{mED}$
508 fusion proteins in these xylem pole pericycle cells should strongly suppress production of lateral
509 roots, phenocopying the solitary root (*slr*) mutant, which carries an auxin-resistant form of IAA14
510 (Fukaki et al., 2002). Indeed, TPLN188 fusion constructs sharply decreased lateral root density
511 (Figure 6E), while transformants expressing either $IAA14^{mED}$ (with no TPL fusion) or TPLN188
512 (with no IAA14 fusion) had no effect on lateral root production (Figure 6E). TPLH3-H9
513 decreased lateral root density albeit not as effectively as TPLN188, suggesting that Helix 1 is
514 required for full repression in a native context (Figure 6E). Both LDimer and Monomer
515 constructs (Figure 6E) were able to repress lateral root development to the same extent as
516 TPLN188, meaning that multimer formation is not required for TPL-mediated repression in this

517 context. The fusion containing the Helix 8 quadruple mutant demonstrated a clear loss of
518 repression, indicating that the TPL-MED21 interaction is critical for repression when expressed
519 in lateral root forming cells (Figure 6E).
520 Given this result, we wanted to directly test the role of AtMed21 in auxin-regulated
521 development in the presence of native isoforms of TPL and Aux/IAAs. This was complicated by
522 the fact that, as in yeast, AtMED21 is essential in plants. While homozygous loss-of-function
523 mutations are embryo lethal (Dhawan et al., 2009), plants heterozygous for *Atmed21* mutations
524 appear wild-type (Figure 6 – Figure Supplement 2A-B). To overcome this obstacle, we took two
525 approaches that relied on the same xylem pole pericycle driver as described for the TPL
526 functional assays. First, we expressed N-terminal deletion variants of MED21 that should
527 weaken or sever interaction with TPL (Figure 6F - Δ3MED21, Δ5 MED21, Δ7 MED21). If
528 MED21-TPL interaction is critical to maintain normal expression of the lateral root program,
529 reduced interaction should trigger an increase in lateral root density. This was exactly what we
530 observed for transgenic lines expressing any of the three deletions. Second, we repressed
531 transcription of *AtMED21* by introducing a dCAS9-TPLN300 synthetic repressor under the
532 control of a UAS promoter along with three sgRNAs complementary to the *AtMED21* promoter.
533 Similar to the predictions above, reduced expression of AtMED21 in xylem pole pericycle cells
534 should stimulate lateral root development. This is indeed what we observed (Figure 6 – Figure
535 Supplement 2C-E).
536 Previous reports connected the Mediator kinase module, and specifically the function of
537 AtMED13/ GRAND CENTRAL (GCT), to repression by TPL (Ito et al., 2016). We did not find
538 evidence for this relationship in our yeast assays, and wanted to investigate further. Although
539 embryo lethality is seen in the majority of homozygous *med13/gct* individuals, a small
540 percentage do survive. This made it possible to examine the effect of expressing wild type and
541 monomeric forms of TPLN188 in xylem pole pericycle cells in the absence of MED13/GCT
542 activity (Figure 6 – Figure Supplement 1E-F). Loss of *med13* function was unable to rescue the
543 production of lateral roots in these lines, leading to the conclusion that TPLN188 requires
544 AtMED21 but not AtMED13 for repression, at least in this context.
545

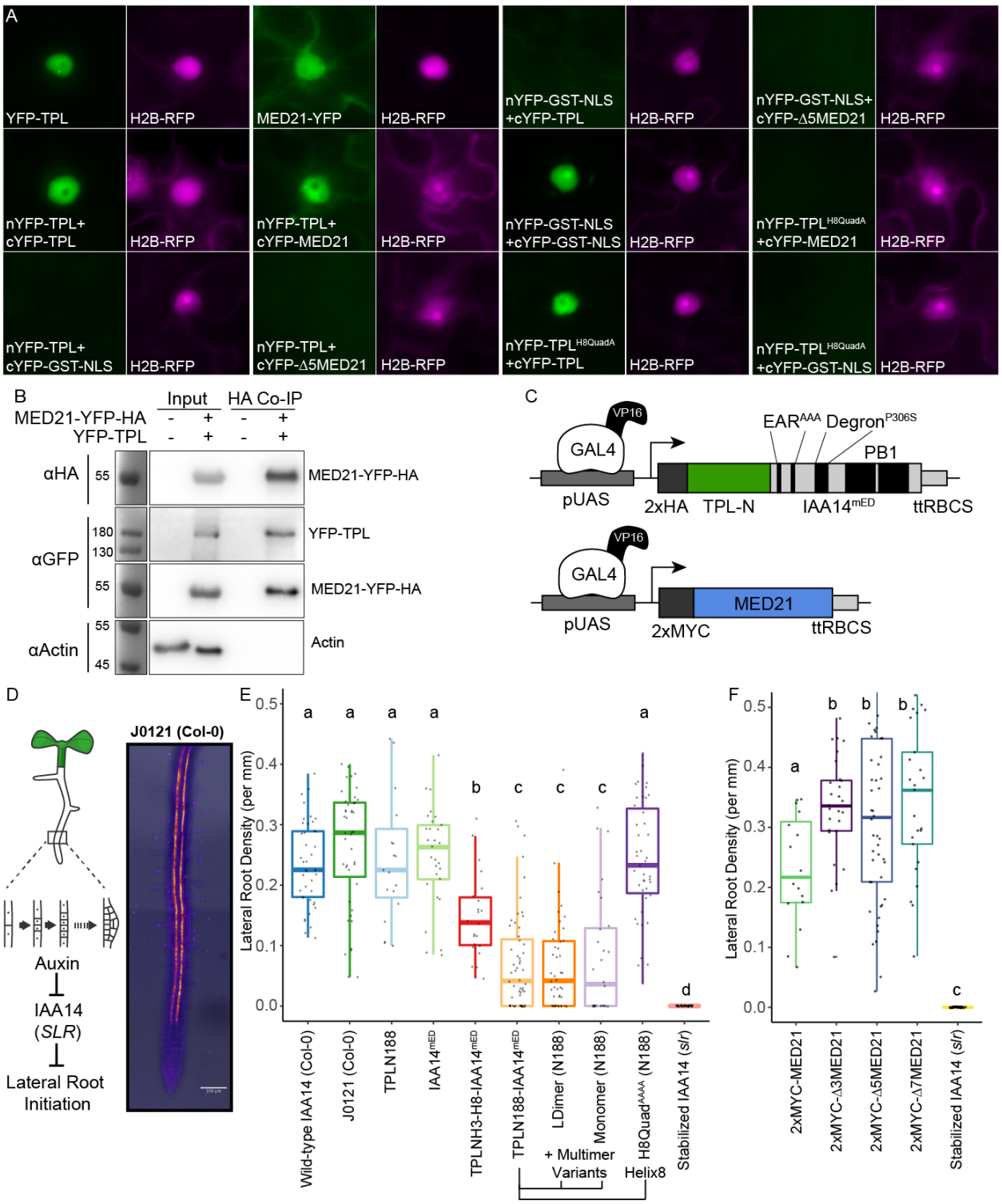

Figure 6. The TPL CRA repression domain behaves similarly in yeast and plants

A. Bimolecular Fluorescence Complementation assay performed in tobacco. Each image is an epi-fluorescent micrograph taken at identical magnification from tobacco epidermal cells at two days post injection. The YFP image is colored green (left panel). p35S:H2B-RFP was used as a

551 control and is false colored magenta (right panel). **B.** Co-immunoprecipitation of MED21 and
552 TPL from tobacco leaves. MED21-YFP-HA was immunoprecipitated using anti-HA, and YFP-
553 TPL was detected using the YFP fusion. Actin was used to demonstrate that the purification had
554 removed non-specific proteins. Numbers on the left of blots indicate sizes of protein standards
555 in kilodaltons. **C.** Design of UAS-TPL-IAA14^{mED} and UAS-MED21 constructs. Mutation of the
556 conserved Lysine residues in the EAR domain disrupted potential interactions with endogenous
557 TPL/TPR proteins. The IAA14 degron has been mutated (P306S) to render it auxin insensitive.
558 UAS – upstream activating sequence, ttRBCS - Rubisco terminator sequence. **D.** Auxin induced
559 degradation of IAA14 is absolutely required for initiation of lateral root development (cartoon,
560 left). An enhancer trap line (J0121) expresses GAL4-VP16 and UAS-GFP in in xylem pole
561 pericycle cells. **E.** N-terminal domains of TPL were sufficient to repress the development of
562 lateral roots in *Arabidopsis* seedlings. The density of emerged lateral roots was measured in T1
563 seedlings at 14 days after germination. **F.** N-terminal deletions in *AtMED21* were sufficient to
564 dominantly increase the development of lateral roots in *Arabidopsis* seedlings. The density of
565 emerged lateral roots was measured in T1 seedlings at 14 days after germination. **F-G**. Lower
566 case letters indicate significant difference (ANOVA and Tukey HSD multiple comparison test;
567 $p<0.001$).
568

569 **Discussion**

570 A review of the current literature on corepressors gives the conflicting impressions that (a)
571 corepressor function is broadly conserved, and (b) that every organism (and perhaps even
572 every corepressor) has a distinct mode for transcriptional repression (Adams et al., 2018; Mottis
573 et al., 2013; Perissi et al., 2010; Wong and Struhl, 2011). We hoped that the *At*ARC^{Sc} could
574 facilitate a resolution to this apparent contradiction by targeting repression to a single synthetic
575 locus. We focused our initial efforts on the analysis of the N-terminal portion of TPL which has
576 multiple known protein-protein interaction surfaces (Ke et al., 2015; Martin-Arevalillo et al.,
577 2017). Experiments with the *At*ARC^{Sc} identified two independent repression domains (Figure 1),
578 and we focused additional study on the stronger of the two localized to the CRA domain. Within
579 this domain, we were able to identify two interacting partners that are part of the middle domain
580 of the Mediator complex: MED21 and MED10 (Figure 2). Four amino acids within Helix 8 with R-
581 groups oriented away from the hydrophobic core of the TPL structure were found to be required
582 for both Med21-binding and repressive function (Figure 3). Indeed, the entire core Mediator
583 complex (Head, Middle, Tail) appears to be recruited to TPL-repressed loci and required to
584 maintain repression (Figure 4). Contrary to our initial hypothesis, the monomeric form of TPL

585 was sufficient for strong repression in yeast and in plants (Figure 5), leaving open the question
586 of the role of higher-order TPL complex formation. Finally, we were able to confirm that our
587 insights from synthetic assays in yeast were relevant to regulation of the auxin-mediated lateral
588 root development pathway in intact plants (Figure 6).

589 Corepressors coordinate multiple mechanisms of repression through discrete protein
590 interactions, leading to robust control over eukaryotic transcription by combining repression
591 modalities. Corepressor function has variously been linked to (a) altering chromatin
592 confirmation, often through interaction with histone modifying proteins or histone proteins
593 themselves, (b) direct interference with transcription factor binding or function, and (c) physical
594 spreading of long-range oligomeric corepressor complexes across regions of regulatory DNA
595 (Perissi et al., 2010). Dissection of the importance of each modality in Tup1 repression has
596 been challenging (Lee et al., 2000; Zhang and Reese, 2004). The tour-de-force of corepressor
597 mechanism studies in yeast concluded that the primary function of Tup1 was to physically block
598 activators (Wong and Struhl, 2011). In their work, the authors utilized the Anchor Away
599 approach to correlate the importance of HDACs, transcriptional machinery and chromatin
600 remodeling enzymes to the repression state of endogenously repressed Cyc8-Tup1 target
601 genes. They observed that Tup1 did not block the binding of transcription factors but inhibited
602 the recruitment of one Mediator component in the tail domain, GAL11/MED15, as well as Pol-II
603 and the chromatin remodelers Snf2 and Sth1. They additionally observed that HDACs had only
604 a supportive role in reinforcing Tup1 repression. These results led to their hypothesis that Tup1
605 blocks the activation domains of transcription factors, and suggested this was through direct
606 binding to activation domains (Wong and Struhl, 2011).

607 The synthetic system used here allowed us to build on this model and further refine our
608 understanding of TPL's repressive activity. In our experiments we see a similar set of
609 conditions, with TPL recruited to the DNA-bound transcriptional activator (ARF), and several
610 possible mechanisms of repression. Unlike Tup1, we have subdivided the TPL protein to identify
611 interactions between TPL and individual protein interactors with no effect on yeast function. In
612 these experiments we can eliminate the possibility that TPL blocks ARF activation by directly
613 blocking the transcription factor activation domains because we see a loss of repression only
614 when TPL-MED21 binding is eliminated through specific point mutations (Figure 4J-L). Our
615 inducible swap of MED21 isoforms also corroborates these findings (Figure 4 – Figure
616 Supplement 3), as the SPARC remains genetically identical in these strains, indicating that TPL-

617 MED21 interaction is regulating Mediator activity not a TPL-ARF interaction. Furthermore, our
618 results correlate well with findings that repressed targets are reactivated when this portion of
619 MED21 is deleted in yeast (TPL - Figure 4, Tup1 - (Gromöller and Lehming, 2000)). Therefore,
620 we suggest that instead of directly binding activation domains that TPL (and likely Tup1) binds
621 to components of Mediator (MED21, MED10B and possibly others) recruited by the transcription
622 factor. Indeed, it is easier to rationalize that the repressor binds the same domains of the
623 Mediator complex recruited by the transcription factor's activation domain (with the same
624 affinity) as opposed to binding each diverse activation domain (with varying affinity). In this
625 model, corepressor binding blocks formation of a fully active Mediator complex thereby limiting
626 Polymerase II recruitment and promoter escape (Petrenko et al., 2017).
627 The Mediator complex is a multi-subunit complex that connects DNA-bound transcription
628 factors and the RNA polymerase II complex (Pol-II) to coordinate gene expression (Flanagan et
629 al., 1991; Kim et al., 1994). The yeast Mediator subunits are organized into four separate
630 modules; head, middle, tail and kinase, with a strong conservation of module components in
631 plants (Dolan and Chapple, 2017; Maji et al., 2019; Malik et al., 2017; Samanta and Thakur,
632 2015). Med21 forms a heterodimer with Med7 to and interacts with Med10, among others, to
633 create the central region of the Middle region of the Mediator complex. The Med21 N-terminus
634 is centered on a flexible hinge region (Baumli et al., 2005), which is required for Pol-II
635 recruitment and CDK8 kinase module recruitment (Sato et al., 2016). The protein interaction
636 between TPL and MED21 occurs at the N-terminus of MED21, highlighting the importance of
637 this region as a signaling hub (Sato et al., 2016). Other lines of evidence support this role, as
638 this region binds the yeast homolog of TPL, Tup1 (Gromöller and Lehming, 2000) through a
639 completely different protein domain as no homology can be found between TPL Helix 8 and
640 Tup1 in any region by primary amino acid homology (i.e. BLAST).
641 As suggested by Ito and colleagues (Ito et al., 2016) and supported by our synthetic
642 system, auxin-induced removal of TPL is sufficient to induce changes in the composition of the
643 Mediator complex; however, multiple points of contact likely exist between the Mediator complex
644 and other parts of the transcriptional machinery in both transcriptionally repressed and active
645 states. For auxin response, specifically, there are several lines of evidence to support this
646 model, including documented association between the structural backbone of Mediator, MED14,
647 and activated and repressed auxin loci in *Arabidopsis* (Ito et al., 2016). In addition, MED12 and
648 MED13 are required for auxin-responsive gene expression in the root, and MED12 acts

649 upstream of AUX1 in the root growth response to sugar (Raya-González et al., 2018). MED18 in
650 the head module represses auxin signaling and positively regulates the viability of the root
651 meristem (Raya-González et al., 2018). PFT1/MED25 regulates auxin transport and response in
652 the root (Raya-González et al., 2014). MED7, MED21's partner protein in the hinge domain, is
653 required for normal root development and loss of MED7 function impacts expression of auxin
654 signaling components (Kumar et al., 2018). Previous research identified the Mediator CDK8
655 subunit, specifically MED13 (MAB2), as an interactor with the full-length TPL protein (Ito et al.,
656 2016). We could not observe interaction between the N-terminal domain of TPL and AtMED13,
657 AtCYC8, or AtCYCC (Supplemental Figure 1B), suggesting that any direct interactions occur
658 outside the N-terminal region.
659 The conserved interaction of both TPL and Tup1 with Mediator has implications for
660 modeling eukaryotic transcription (e.g., (Estrada et al., 2016)). By stabilizing the Mediator
661 complex, TPL (and by extension Tup1) may create a 'pre-paused' state that allows rapid
662 recruitment of Pol-II and activation once TPL is removed. This would be compatible with the
663 multiple repression mechanisms have been described for TPL at different genetic loci. TPL
664 recruitment of the repressive CDK8 Mediator complex (Ito et al., 2016), chromatin remodeling
665 enzymes such as Histone Deacetylase 19 (HD19) (Long et al., 2006) and contact with histone
666 proteins (Ma et al., 2017) would be removed with TPL upon relief of repression. It will be critical
667 in the future to understand how these various forms of repression interact, and especially to
668 map the dynamics of assembly and disassembly of complexes as loci transition from repressed
669 to active states and back to repressed once again.

670 **RESOURCE AVAILABILITY**

671 ***Lead Contact***

672 Further information and requests for resources and reagents should be directed to and will be
673 fulfilled by the Lead Contact, Jennifer, Nemhauser (jn7@uw.edu).

674 ***Materials Availability***

675 Plasmids generated in this study will be deposited to [Addgene, Jennifer Nemhauser].

676 ***Data and Code Availability***

677 *Data and Code Availability Statement*

678 All flow cytometry data is deposited at https://flowrepository.org/. Repository IDS:
679 FR-FCM-Z2GM, FR-FCM-Z2GR, FR-FCM-Z2GQ, FR-FCM-Z2GX, FR-FCM-Z2GT, FR-
680 FCM-Z2W2.

681 All protein interactions will be deposited at IntAct.

682 All code is available through Github:
683 https://github.com/achillobator/TPL_Structure_Function/

684

685 **Method Details**

686 **Cloning**

687 Construction of TPL-IAA3 and TPL-IAA14 fusion proteins were performed by golden gate
688 cloning as described in (Pierre-Jerome et al., 2014). Variant and deletion constructs were
689 created using PCR-mediated site-directed mutagenesis. Site-directed mutagenesis primers
690 were designed using NEBasechanger and implemented through Q5® Site-Directed
691 Mutagenesis (NEB, Cat #E0554S). TPL interactor genes were amplified as cDNAs from wild
692 type Col-0 RNA using reverse transcriptase (SuperScript™ IV Reverse Transcriptase,
693 Invitrogen) and gene-specific primers from IDT (Coralville, Iowa), followed by amplification with
694 Q5 polymerase (NEB). These cDNAs were subsequently cloned into Plasmids for cytoSUS
695 using a Gibson approach (Gibson et al., 2009), through the Aquarium Biofabrication facility (Ben
696 Keller et al., 2019). The coding sequence of the genes of interest were confirmed by sequencing
697 (Genewiz; South Plainfield, NJ). For UAS driven constructs, the TPLN188-IAA14 coding
698 sequence was amplified with primers containing engineered BsaI sites and introduced into the
699 pGII backbone with the UAS promoter and RBSC terminator (Siligato et al., 2016) using Golden
700 Gate cloning (Weber et al., 2011). Subsequent mutations were performed on this backbone
701 using PCR-mediated site-directed mutagenesis (see above). Construction of C-terminal 2xFRB

702 fusions for Anchor Away were constructed as described in (Haruki et al., 2008). Inducible
703 MED21 was constructed as described in (McIsaac et al., 2013). For cell type specific
704 knockdown mediated by dCas9-TPLN300, Gibson cloning was used modify the pHEE401E
705 plasmid, replacing the egg-specific promoter and Cas9 from pHEE401E (Wang et al., 2015) with
706 UAS promoter and dCas9- TPLN300 fusion protein (Khakhar et al., 2018). The resulting plasmid
707 is used as starting point to clone 3 sgRNAs targeting the *AtMED21* promoter (identified using
708 CHOP CHOP (Labun et al., 2019). sgRNAs: GACGCAGAGTCTGTTGGGTGTGG,
709 TTTAAAATGGGCTTTTAAGGTGG, AACACTGAAGTAGAATTGGGTGG ranging from -170 to
710 +90 region from the TSS) using PCR and Golden Gate cloning strategy described in (Wang et
711 al., 2015).
712
713 **Flow Cytometry**
714 Fluorescence measurements were taken using a Becton Dickinson (BD) special order
715 cytometer with a 514-nm laser exciting fluorescence that is cut off at 525 nm prior to
716 photomultiplier tube collection (BD, Franklin Lakes, NJ). Events were annotated, subset to
717 singlet yeast using the FlowTime R package (Wright et al., 2019). A total of 10,000 - 20,000
718 events above a 400,000 FSC-H threshold (to exclude debris) were collected for each sample
719 and data exported as FCS 3.0 files for processing using the flowCore R software package and
720 custom R scripts (Supplemental File 1, (Havens et al., 2012; Pierre-Jerome et al., 2017)). Data
721 from at least two independent replicates were combined and plotted in R (ggplots2).
722
723 **Yeast Methods**
724 Standard yeast drop-out and yeast extract–peptone–dextrose plus adenine (YPAD) media were
725 used, with care taken to use the same batch of synthetic complete (SC) media for related
726 experiments. A standard lithium acetate protocol (Gietz and Woods, 2002) was used for
727 transformations of digested plasmids. All cultures were grown at 30°C with shaking at 220 rpm.
728 Anchor-Away approaches were followed as described in (Haruki et al., 2008), and anchor away
729 strains were obtained from EURO-SCARF (euroscarf.de). Endogenous genomic fusions of
730 ScMed21-FRB were designed by fusing MED21 homology to the pFA6a-FRB-KanMX6 plasmid
731 for chromosomal integration into the parental anchor away strain as in (Petrenko et al., 2017),
732 selectable through G418 resistance (G418, Geneticin, Thermo Fisher Scientific). Tup1-FRB and
733 Cyc8-FRB were constructed as described in (Wong and Struhl, 2011). Mediator anchor away

734 strains were created in (Petrenko et al., 2017) and kindly donated by Dr. Kevin Struhl. SPARC
735 construction required a redesign of promoters and terminators used in the *At*ARC^{Sc} to eliminate
736 any repetitive DNA sequences (See Figure 4 – Figure Supplement 1), using a Golden Gate
737 cloning approach into level 1 vectors. Subsequent assembly of individual transcriptional units
738 into a larger plasmid utilized VEGAS assembly which was performed as described in (Mitchell et
739 al., 2015). To create an acceptor plasmid for the assembled transcriptional units, we
740 synthesized a custom vector containing VA1 and VA2 homology sites for recombination (Twist
741 Bioscience, South San Francisco, CA). In between these sites we incorporated a pLac:mRFP
742 cassette to allow identification of uncut destination plasmid in *E. coli*, flanked by EcoRI sites for
743 linearization. Finally, the CEN6/ARSH4 was transferred from pRG215 (Addgene #64525) into
744 the acceptor plasmid by Golden Gate reaction using designed BsmBI sites engineered into the
745 acceptor plasmid and the primers used to amplify the CEN/ARS (See Figure 4 – Figure
746 Supplement 1). For the cytoplasmic split-ubiquitin protein-protein interaction system, bait and
747 prey constructs were created using the plasmids pMetOYC and pNX32, respectively (Addgene,
748 https://www.addgene.org/Christopher_Grefen/). Interaction between bait and prey proteins were
749 evaluated using a modified version of the split ubiquitin technique (Asseck and Grefen, 2018).
750 After two days of growth on control and selection plates, images were taken using a flatbed
751 scanner (Epson America, Long Beach, CA). Inducible ScMed21 strains (iMed21) were grown
752 overnight, and then diluted back to 100 events per microliter as determined by flow cytometry
753 and grown at 30C with 250rpm in a deepwell 96-well plate format. Strains were supplemented
754 with β-estradiol (20μM) for 4 hours followed by Rapamycin addition. Samples were analyzed by
755 flow cytometry throughout these growth experiments.
756
757 **Western Blot**
758 Yeast cultures that had been incubated overnight in synthetic complete (SC) media were diluted
759 to OD600 = 0.6 and incubated until cultures reached OD600 ~1. Cells were harvested by
760 centrifugation. Cells were lysed by vortexing for 5 min in the presence of 200 μl of 0.5-mm
761 diameter acid washed glass beads and 200 μl SUMEB buffer (1% SDS, 8 M urea, 10 mM
762 MOPS pH 6.8, 10 mM EDTA, 0.01% bromophenol blue, 1mM PMSF) per one OD unit of original
763 culture. Lysates were then incubated at 65° for 10 min and cleared by centrifugation prior to
764 electrophoresis and blotting. Antibodies: Anti-HA-HRP (REF-12013819001, Clone 3F10,
765 Roche/Millipore Sigma, St. Louis, MO), Anti-FLAG (F3165, Monoclonal ANTI-FLAG® M2,

766 Millipore Sigma, St. Louis, MO), Anti-FRB (ALX-215-065-1, Enzo Life Sciences, Farmingdale,
767 NY, (Haruki et al., 2008)), Anti-VP16 (1-21) (sc-7545, Santa Cruz Biotechnology, Dallas TX),
768 Anti-GFP (ab290, AbCam, Cambridge, United Kingdom), Anti-MYC (71d10, 2278S, Cell
769 Signaling, Danvers, MA), Anti-PGK1 (ab113687, AbCam, Cambridge, United Kingdom).
770
771 **Protein expression and purification**
772 All multimer deficient TPL proteins were expressed in *Escherichia coli* Rosetta 2 strain. Bacteria
773 cultures were grown at 37ºC until they achieved an OD^{600}nm of 0.6-0.9. Protein expression was
774 induced with isopropyl-β-D-1-thyogalactopiranoside (IPTG) at a final concentration of 400 µM at
775 18 °C overnight. Bacteria cultures were centrifuged and the pellets were resuspended in the
776 buffer A (CAPS 200 mM pH 10.5, NaCl 500 mM, TCEP 1 mM), where cells were lysed by
777 sonication. His-tagged AtTPL188 (wt and mutants) bacteria pellets were resuspended in buffer
778 A with EDTA-free antiprotease (Roche). The soluble fractions recovered after sonication were
779 passed through a Ni-sepharose (GE Healthcare) column previously washed with buffer A and
780 the bound proteins were eluted with buffer A with 250 mM imidazole. A second purification step
781 was carried out on Gel filtration Superdex 200 10/300 GL (GE Healthcare) equilibrated with
782 buffer A.
783
784 **Co-Immunoprecipitation**
785 Co-IP from yeast was performed using the cytoSUS strains. Cultures were grown to OD600 0.5
786 (~1E7 cells/ml) using selective media, harvested, and resuspended in 200 µl SUME (1% SDS,
787 8M Urea, 10mM MOPS, pH 6.8, 10mM EDTA) buffer with protease inhibitors. Cells were lysed
788 by vortexing 3 X 1 min full speed with 100 µl of 0.5 mm Acid Washed Glass Beads, clarified by
789 centrifugation (1 min, 1000rpm), and supernatant was mixed with 1ml IP buffer (15mM
790 Na2HPO4, mw 142; 150mM NaCl, mw 58; 2% Triton X-100, 0.1% SDS, 0.5% DOC, 10mM
791 EDTA, 0.02% NaN3) with protease inhibitors, and incubated with 100 µl of IgG sepharose at
792 25°C for 2 hours with rotation. The Beads were washed 1x with IP buffer, and 2x with IP-Wash
793 buffer (50mM NaCl, mw58; 10mM TRIS, mw 121; 0.02% NaN3) with protease inhibitors. Protein
794 was eluted with 50 µl of SUME buffer + 0.005% bromophenol blue by incubation at 65°C for 10
795 minutes and run on handmade 12% acrylamide SDS-PAGE gels, and western blotted
796 accordingly. Co-IPs from tobacco were performed on leaves two days after injection as
797 described in (Song et al., 2014), using 35S:MED21-YFP-HA, 35S:TPL-YFP (full length), and

798 35S:MED10B-MEC-ProtA constructs. For Co-IPs with HA, extracts were incubated with Anti-
799 HA-Biotin (High Affinity (3F10), Sigma, 12158167001) and Streptavidin conjugated magnetic
800 beads (Life Technologies, Dynabeads M-280 Streptavidin, 112.05D). For Co-IPs with MED10B-
801 MEC-ProtA we used IgG Sepharose® 6 Fast Flow (Sigma, GE17-0969-01) beads and
802 increased washing steps (1xIP buffer, 4xWash buffer, 5 total). The only modification to buffers
803 was an addition of the detergent NP-40 at 0.1% in the IP and wash buffer. Samples were run on
804 handmade 10% acrylamide SDS-PAGE gels, and western blotted accordingly.
805
806 **Bimolecular Fluorescence Complementation (BiFC)**
807 Bimolecular fluorescent complementation experiments were performed on 3-week-old *N.*
808 *benthamiana* plants grown at 22°C under long days (16 h light/8 h dark) on soil (Sunshine #4
809 mix) as per (Martin et al., 2009). pSITE vectors were used to generate BiFC constructs for
810 MED21, Δ5-MED21, TPL and $TPL^{H8QuadA}$ – proteins (Martin et al., 2009). In all cases the
811 combinations are N-terminal fusions of either the nEYFP or cEYFP to the cDNA of MED21 or
812 TPL. RFP fused Histone H2B was used as a nuclear marker (Goodin et al., 2002). Injection of
813 Agrobacterium strains into tobacco leaves was performed as in (Goodin et al., 2002), but the
814 OD_{600} of the Agrobacterium culture used was adjusted to 0.5. Two days after transfection, plant
815 leaves were imaged using an epifluorescence microscope (Leica Biosystems, model: DMI
816 3000B).
817
818 **Chromatin Immunoprecipitation.**
819 Yeast were inoculated in liquid YPD and grown at 30 °C with shaking at 225 rpm. After 18 h of
820 growth, cultures were diluted 1:50 in fresh YPD to a final volume of 200 mL. Four hours post-
821 dilution, cells were treated with 20 mL of fix solution [11% (vol/vol) formaldehyde, 0.1 M NaCl, 1
822 mM EDTA, 50 mM Hepes–KOH] for 20 min at room temperature with shaking. Cultures were
823 further treated with 36 mL of 2.5 M glycine for 5 min to quench the cross-linking. Cells were then
824 pelleted at 4°C, washed twice with ice-cold TBS, and flash-frozen in liquid nitrogen. Cells were
825 lysed in breaking buffer [100 mM Tris, pH 8.0, 20% (vol/vol) glycerol, and 1 mM PMSF] on a
826 bead beater before sonication. Samples were processed in a Bioruptor Plus sonication device at
827 50% for 30 cycles. Following centrifugation (to pellet cellular debris), the supernatant was used
828 for the IP reaction. Biotin conjugated Anti-HA (High Affinity (3F10), Sigma, 12158167001)
829 coupled to Streptavidin coated Dynabeads Streptavidin conjugated magnetic beads (Life

830 Technologies, Dynabeads M-280 Streptavidin, 112.05D) was used to probe for HA-tagged
831 TPLN188. Anti-FRB coupled to Protein A Dynabeads (Life Technologies, 100.02D). Following
832 elution from the beads, samples were incubated overnight at 65 °C to reverse cross-links. DNA
833 was purified using a Monarch PCR purification kit (NEB). qPCR for three independent replicates
834 was performed using iQ SYBR Green Supermix (Biorad) in a C100 thermocycler fitted with a
835 CFX96 Real-Time Detection System (Biorad).
836
837 **Protein alignments**
838 The MED21 protein sequence was were aligned to homologs using CLC Sequence Viewer 7, a
839 tree was constructed using a Neighbor-Joining method, and bootstrap analysis performed with
840 10,000 replicates.
841
842 **Plant growth**
843 For synthetic repression assays in tobacco Agrobacterium-mediated transient transformation of
844 *Nicotiana benthamiana* was performed as per (Yang et al., 2000). 5 ml cultures of
845 Agrobacterium strains were grown overnight at 30C shaking at 220rpm, pelleted and incubated
846 in MMA media (10 mM MgCl2, 10 mM MES pH 5.6, 100 µM acetosyringone) for 3 hours at room
847 temperature with rotation. Strain density was normalized to an OD600 of 1 for each strain in the
848 final mixture of strains before injection into tobacco leaves. Leaves were removed, and 8
849 different regions were excised using a hole punch, placed into a 96-well microtiter plate with
850 100µl of water. Each leaf punch was scanned in a 4x4 grid for yellow and red fluorescence
851 using a plate scanner (Tecan Spark, Tecan Trading AG, Switzerland). Fluorescence data was
852 quantified and plotted in R (ggplots). For *Arabidopsis thaliana* experiments using the GAL4-
853 UAS system (Laplaze et al., 2005), J0121 was introgressed eight times into Col-0 accession
854 from the C24 accession, and rigorously checked to ensure root growth was comparable to Col-0
855 before use. UAS-TPL-IAA14^{mED} constructs were introduced to J0121 introgression lines by floral
856 dip method (Clough and Bent, 1998). T1 seedlings were selected on 0.5X LS (Caisson
857 Laboratories, Smithfield, UT) + 25µg/ml Hygromycin B (company) + 0.8% phytoagar
858 (Plantmedia; Dublin, OH). Plates were stratified for 2 days, exposed to light for 6 h, and then
859 grown in the dark for 3 d following a modification of the method of (Harrison et al., 2006).
860 Hygromycin resistant seedlings were identified by their long hypocotyl, enlarged green leaves
861 and long root. Transformants were transferred by hand to fresh 0.5X LS plates + 0.8% Bacto

agar (Thermo Fisher Scientific) and grown vertically for 14 days at 22°C. Plates were scanned on a flatbed scanner (Epson America, Long Beach, CA) at day 14. *slr* and *med21/MED21* (WiscDsLox461-464K13) seeds were obtained from the Arabidopsis Biological Resource Center (Columbus, OH). CRISPR/CAS9 based mutations in AtMED2 were generated as described in (Wang et al., 2015). We created a novel mutation in *AtMED21* that introduces a single base-pair insertion of G at nucleotide 214 after the A of the start codon (i214G). This mutation alters the amino acid sequence starting at residue 25 and creates an early stop codon after 11 random amino acids (Supplemental Figure 6D).

Data submissions

All flow cytometry data will be deposited at https://flowrepository.org/. All plasmids will be deposited through Addgene at https://www.addgene.org/Jennifer_Nemhauser/.

Acknowledgements

We would like to thank Prof. Jef Boeke for kindly providing VEGAS adaptor and regulatory element plasmids; Dr. Jennifer Brophy and Prof. José Dinneny for kindly providing the pUBQ10:GAL4:VP16 plasmid; Dr. Natalia Petrenko and Dr. Kevin Struhl for kindly providing Mediator anchor away strains; and Prof. Grant Brown and Prof. Maitreya Dunham for advice on yeast genetics and approaches. We thank members of the Nemhauser group including Amy Lanctot, Romi Ramos, Eric Yang, and Dr. Sarah Guiziou for constructive discussions and comments on this manuscript. We also thank Morgan Hamm for the custom R script used here to analyze anchor away plates.

Author Contributions

Conceptualization: ARL, JLN; Investigation: ARL, WW, HPG, SG, SJS, MLZ, JEZ; Software: ARL, HPG; Formal Analysis: ARL, HPG; Visualization: ARL, WW, HPG, SG, SJS, MLZ, JEZ; Writing-Original Draft: ARL; Writing-Review & Editing: WW, HPG, SG, SJS, MLZ, JEZ, NZ, JLN; Supervision, Project administration, Funding Acquisition, Resources: JLN, NZ.

Declaration of Interests

The authors declare no competing interests.

Funding

National Institutes of Health (NIH): ARL, HPG, SG, SJS, JEZ, MZ & JLN R01- GM107084.

Howard Hughes Medical Institute (HHMI): ARL, SJS, JEZ, MZ & JLN - Faculty Scholar Award.

Ning Zheng is a Howard Hughes Medical Institute Investigator.

ARL is supported by the Simons Foundation through the Life Science Research Foundation.

900 **References**

901 Adams GE, Chandru A, Cowley SM. 2018. Co-repressor, co-activator and general transcription
902 factor: the many faces of the Sin3 histone deacetylase (HDAC) complex. *Biochem J*
903 **475**:3921–3932. doi:10.1042/BCJ20170314
904 Agarwal M, Kumar P, Mathew SJ. 2015. The Groucho/Transducin-like enhancer of split protein
905 family in animal development. *IUBMB Life* **67**:472–481. doi:10.1002/iub.1395
906 Asseck LY, Grefen C. 2018. Detecting Interactions of Membrane Proteins: The Split-Ubiquitin
907 System. *Methods Mol Biol Clifton NJ* **1794**:49–60. doi:10.1007/978-1-4939-7871-7_4
908 Baumli S, Hoeppner S, Cramer P. 2005. A Conserved Mediator Hinge Revealed in the Structure
909 of the MED7·MED21 (Med7·Srb7) Heterodimer. *J Biol Chem* **280**:18171–18178.
910 doi:10.1074/jbc.M413466200
911 Ben Keller, Justin Vrana, Abraham Miller, Garrett Newman, Eric Klavins. 2019. Aquarium: The
912 Laboratory Operating System. Zenodo. doi:10.5281/zenodo.2535715
913 Biddick R, Young ET. 2005. Yeast Mediator and its role in transcriptional regulation. *C R Biol*
914 **328**:773–782. doi:10.1016/j.crvi.2005.03.004
915 Bourbon H-M. 2008. Comparative genomics supports a deep evolutionary origin for the large,
916 four-module transcriptional mediator complex. *Nucleic Acids Res* **36**:3993–4008.
917 doi:10.1093/nar/gkn349
918 Brand AH, Perrimon N. 1993. Targeted gene expression as a means of altering cell fates and
919 generating dominant phenotypes. *Dev Camb Engl* **118**:401–415.
920 Busch W, Miotk A, Ariel FD, Zhao Z, Forner J, Daum G, Suzaki T, Schuster C, Schultheiss SJ,
921 Leibfried A, Haubeiss S, Ha N, Chan RL, Lohmann JU. 2010. Transcriptional control of a
922 plant stem cell niche. *Dev Cell* **18**:849–861. doi:10.1016/j.devcel.2010.03.012
923 Carlson M, Botstein D. 1982. Two differentially regulated mRNAs with different 5' ends encode
924 secreted with intracellular forms of yeast invertase. *Cell* **28**:145–154. doi:10.1016/0092-
925 8674(82)90384-1
926 Causier B, Ashworth M, Guo W, Davies B. 2012. The TOPLESS interactome: a framework for
927 gene repression in Arabidopsis. *Plant Physiol* **158**:423–438. doi:10.1104/pp.111.186999
928 Chen G, Courey AJ. 2000. Groucho/TLE family proteins and transcriptional repression. *Gene*
929 **249**:1–16. doi:10.1016/s0378-1119(00)00161-x
930 Clough SJ, Bent AF. 1998. Floral dip: a simplified method for Agrobacterium-mediated
931 transformation of Arabidopsis thaliana. *Plant J Cell Mol Biol* **16**:735–743.
932 Collins J, O'Grady K, Chen S, Gurley W. 2019. The C-terminal WD40 repeats on the TOPLESS
933 co-repressor function as a protein–protein interaction surface. *Plant Mol Biol* **100**:47–58.
934 doi:10.1007/s11103-019-00842-w
935 Delto CF, Heisler FF, Kuper J, Sander B, Kneussel M, Schindelin H. 2015. The LisH motif of
936 muskelin is crucial for oligomerization and governs intracellular localization. *Struct Lond*
937 *Engl 1993* **23**:364–373. doi:10.1016/j.str.2014.11.016
938 Dhawan R, Luo H, Foerster AM, Abuqamar S, Du H-N, Briggs SD, Mittelsten Scheid O,
939 Mengiste T. 2009. HISTONE MONOUBIQUITINATION1 interacts with a subunit of the
940 mediator complex and regulates defense against necrotrophic fungal pathogens in
941 Arabidopsis. *Plant Cell* **21**:1000–1019. doi:10.1105/tpc.108.062364
942 Dolan WL, Chapple C. 2017. Conservation and Divergence of Mediator Structure and Function:
943 Insights from Plants. *Plant Cell Physiol* **58**:4–21. doi:10.1093/pcp/pcw176
944 Estrada J, Wong F, DePace A, Gunawardena J. 2016. Information Integration and Energy
945 Expenditure in Gene Regulation. *Cell* **166**:234–244. doi:10.1016/j.cell.2016.06.012
946 Flanagan PM, Kelleher RJ, Sayre MH, Tschochner H, Kornberg RD. 1991. A mediator required
947 for activation of RNA polymerase II transcription in vitro. *Nature* **350**:436–438.
948 doi:10.1038/350436a0

949 Fleming AB, Pennings S. 2007. Tup1-Ssn6 and Swi-Snf remodelling activities influence long-
950 range chromatin organization upstream of the yeast SUC2 gene. *Nucleic Acids Res*
951 **35**:5520–5531. doi:10.1093/nar/gkm573
952 Flowers EB, Poole RJ, Tursun B, Bashllari E, Pe'er I, Hobert O. 2010. The Groucho ortholog
953 UNC-37 interacts with the short Groucho-like protein LSY-22 to control developmental
954 decisions in C. elegans. *Dev Camb Engl* **137**:1799–1805. doi:10.1242/dev.046219
955 Fukaki H, Tameda S, Masuda H, Tasaka M. 2002. Lateral root formation is blocked by a gain-
956 of-function mutation in the SOLITARY-ROOT/IAA14 gene of Arabidopsis. *Plant J Cell*
957 *Mol Biol* **29**:153–168.
958 Gala HP, Lanctot A, Jean-Baptiste K, Guiziou S, Chu JC, Zemke JE, George W, Queitsch C,
959 Cuperus JT, Nemhauser JL. 2020. A single cell view of the transcriptome during lateral
960 root initiation in Arabidopsis thaliana. *bioRxiv* 2020.10.02.324327.
961 doi:10.1101/2020.10.02.324327
962 Gasperowicz M, Otto F. 2005. Mammalian Groucho homologs: redundancy or specificity? *J Cell*
963 *Biochem* **95**:670–687. doi:10.1002/jcb.20476
964 Gibson DG, Young L, Chuang R-Y, Venter JC, Hutchison CA, Smith HO. 2009. Enzymatic
965 assembly of DNA molecules up to several hundred kilobases. *Nat Methods* **6**:343–345.
966 doi:10.1038/nmeth.1318
967 Gietz RD, Woods RA. 2002. Transformation of yeast by lithium acetate/single-stranded carrier
968 DNA/polyethylene glycol method. *Methods Enzymol* **350**:87–96. doi:10.1016/s0076-
969 6879(02)50957-5
970 Gonzalez N, Pauwels L, Baekelandt A, De Milde L, Van Leene J, Besbrugge N, Heyndrickx KS,
971 Cuéllar Pérez A, Durand AN, De Clercq R, Van De Slijke E, Vanden Bossche R,
972 Eeckhout D, Gevaert K, Vandepoele K, De Jaeger G, Goossens A, Inzé D. 2015. A
973 Repressor Protein Complex Regulates Leaf Growth in Arabidopsis. *Plant Cell* **27**:2273–
974 2287. doi:10.1105/tpc.15.00006
975 Goodin MM, Dietzgen RG, Schichnes D, Ruzin S, Jackson AO. 2002. pGD vectors: versatile
976 tools for the expression of green and red fluorescent protein fusions in agroinfiltrated
977 plant leaves. *Plant J Cell Mol Biol* **31**:375–383. doi:10.1046/j.1365-313x.2002.01360.x
978 Grbavec D, Lo R, Liu Y, Stifani S. 1998. Transducin-like Enhancer of split 2, a mammalian
979 homologue of Drosophila Groucho, acts as a transcriptional repressor, interacts with
980 Hairy/Enhancer of split proteins, and is expressed during neuronal development. *Eur J*
981 *Biochem* **258**:339–349.
982 Gromöller A, Lehming N. 2000. Srb7p is a physical and physiological target of Tup1p. *EMBO J*
983 **19**:6845–6852. doi:10.1093/emboj/19.24.6845
984 Hallberg M, Hu G-Z, Tronnersjö S, Shaikhibrahim Z, Balciunas D, Björklund S, Ronne H. 2006.
985 Functional and physical interactions within the middle domain of the yeast mediator. *Mol*
986 *Genet Genomics MGG* **276**:197–210. doi:10.1007/s00438-006-0135-7
987 Harrison SJ, Mott EK, Parsley K, Aspinall S, Gray JC, Cottage A. 2006. A rapid and robust
988 method of identifying transformed Arabidopsis thaliana seedlings following floral dip
989 transformation. *Plant Methods* **2**:19. doi:10.1186/1746-4811-2-19
990 Haruki H, Nishikawa J, Laemmli UK. 2008. The anchor-away technique: rapid, conditional
991 establishment of yeast mutant phenotypes. *Mol Cell* **31**:925–932.
992 doi:10.1016/j.molcel.2008.07.020
993 Havens KA, Guseman JM, Jang SS, Pierre-Jerome E, Bolten N, Klavins E, Nemhauser JL.
994 2012. A synthetic approach reveals extensive tunability of auxin signaling. *Plant Physiol*
995 **160**:135–142. doi:10.1104/pp.112.202184
996 Ito J, Fukaki H, Onoda M, Li L, Li C, Tasaka M, Furutani M. 2016. Auxin-dependent
997 compositional change in Mediator in ARF7- and ARF19-mediated transcription. *Proc*
998 *Natl Acad Sci U S A* **113**:6562–6567. doi:10.1073/pnas.1600739113

999 Kagale S, Links MG, Rozwadowski K. 2010. Genome-wide analysis of ethylene-responsive
1000 element binding factor-associated amphiphilic repression motif-containing transcriptional
1001 regulators in Arabidopsis. *Plant Physiol* **152**:1109–1134. doi:10.1104/pp.109.151704
1002 Ke J, Ma H, Gu X, Thelen A, Brunzelle JS, Li J, Xu HE, Melcher K. 2015. Structural basis for
1003 recognition of diverse transcriptional repressors by the TOPLESS family of corepressors.
1004 *Sci Adv* **1**:e1500107. doi:10.1126/sciadv.1500107
1005 Keleher CA, Redd MJ, Schultz J, Carlson M, Johnson AD. 1992. Ssn6-Tup1 is a general
1006 repressor of transcription in yeast. *Cell* **68**:709–719. doi:10.1016/0092-8674(92)90146-4
1007 Khakhar A, Leydon AR, Lemmex AC, Klavins E, Nemhauser JL. 2018. Synthetic hormone-
1008 responsive transcription factors can monitor and re-program plant development. *eLife* **7**.
1009 doi:10.7554/eLife.34702
1010 Kim MH, Cooper DR, Oleksy A, Devedjiev Y, Derewenda U, Reiner O, Otlewski J, Derewenda
1011 ZS. 2004. The Structure of the N-Terminal Domain of the Product of the Lissencephaly
1012 Gene Lis1 and Its Functional Implications. *Structure* **12**:987–998.
1013 doi:10.1016/j.str.2004.03.024
1014 Kim YJ, Björklund S, Li Y, Sayre MH, Kornberg RD. 1994. A multiprotein mediator of
1015 transcriptional activation and its interaction with the C-terminal repeat domain of RNA
1016 polymerase II. *Cell* **77**:599–608. doi:10.1016/0092-8674(94)90221-6
1017 Klepikova AV, Kasianov AS, Gerasimov ES, Logacheva MD, Penin AA. 2016. A high resolution
1018 map of the Arabidopsis thaliana developmental transcriptome based on RNA-seq
1019 profiling. *Plant J* **88**:1058–1070. doi:10.1111/tpj.13312
1020 Kornberg RD. 2005. Mediator and the mechanism of transcriptional activation. *Trends Biochem*
1021 *Sci* **30**:235–239. doi:10.1016/j.tibs.2005.03.011
1022 Krogan NT, Hogan K, Long JA. 2012. APETALA2 negatively regulates multiple floral organ
1023 identity genes in Arabidopsis by recruiting the co-repressor TOPLESS and the histone
1024 deacetylase HDA19. *Dev Camb Engl* **139**:4180–4190. doi:10.1242/dev.085407
1025 Kumar KRR, Blomberg J, Björklund S. 2018. The MED7 subunit paralogs of Mediator function
1026 redundantly in development of etiolated seedlings in Arabidopsis. *Plant J* **96**:578–594.
1027 doi:10.1111/tpj.14052
1028 Labun K, Montague TG, Krause M, Torres Cleuren YN, Tjeldnes H, Valen E. 2019.
1029 CHOPCHOP v3: expanding the CRISPR web toolbox beyond genome editing. *Nucleic*
1030 *Acids Res* **47**:W171–W174. doi:10.1093/nar/gkz365
1031 Laplaze L, Parizot B, Baker A, Ricaud L, Martinière A, Auguy F, Franche C, Nussaume L,
1032 Bogusz D, Haseloff J. 2005. GAL4-GFP enhancer trap lines for genetic manipulation of
1033 lateral root development in Arabidopsis thaliana. *J Exp Bot* **56**:2433–2442.
1034 doi:10.1093/jxb/eri236
1035 Lee JE, Golz JF. 2012. Diverse roles of Groucho/Tup1 co-repressors in plant growth and
1036 development. *Plant Signal Behav* **7**:86–92. doi:10.4161/psb.7.1.18377
1037 Lee M, Chatterjee S, Struhl K. 2000. Genetic analysis of the role of Pol II holoenzyme
1038 components in repression by the Cyc8-Tup1 corepressor in yeast. *Genetics* **155**:1535–
1039 1542.
1040 Liu X, Galli M, Camehl I, Gallavotti A. 2019. RAMOSA1 ENHANCER LOCUS2-Mediated
1041 Transcriptional Repression Regulates Vegetative and Reproductive Architecture. *Plant*
1042 *Physiol* **179**:348–363. doi:10.1104/pp.18.00913
1043 Liu Z, Karmarkar V. 2008. Groucho/Tup1 family co-repressors in plant development. *Trends*
1044 *Plant Sci* **13**:137–144. doi:10.1016/j.tplants.2007.12.005
1045 Long JA, Ohno C, Smith ZR, Meyerowitz EM. 2006. TOPLESS regulates apical embryonic fate
1046 in Arabidopsis. *Science* **312**:1520–1523. doi:10.1126/science.1123841
1047 Ma H, Duan J, Ke J, He Y, Gu X, Xu T-H, Yu H, Wang Y, Brunzelle JS, Jiang Y, Rothbart SB,
1048 Xu HE, Li J, Melcher K. 2017. A D53 repression motif induces oligomerization of

1049 TOPLESS corepressors and promotes assembly of a corepressor-nucleosome complex.
1050 *Sci Adv* **3**:e1601217. doi:10.1126/sciadv.1601217
1051 Maji S, Dahiya P, Waseem M, Dwivedi N, Bhat DS, Dar TH, Thakur JK. 2019. Interaction map
1052 of Arabidopsis Mediator complex expounding its topology. *Nucleic Acids Res* **47**:3904–
1053 3920. doi:10.1093/nar/gkz122
1054 Malik N, Agarwal P, Tyagi A. 2017. Emerging functions of multi-protein complex Mediator with
1055 special emphasis on plants. *Crit Rev Biochem Mol Biol* **52**:475–502.
1056 doi:10.1080/10409238.2017.1325830
1057 Martin K, Kopperud K, Chakrabarty R, Banerjee R, Brooks R, Goodin MM. 2009. Transient
1058 expression in Nicotiana benthamiana fluorescent marker lines provides enhanced
1059 definition of protein localization, movement and interactions in planta. *Plant J Cell Mol*
1060 *Biol* **59**:150–162. doi:10.1111/j.1365-313X.2009.03850.x
1061 Martin-Arevalillo R, Nanao MH, Larrieu A, Vinos-Poyo T, Mast D, Galvan-Ampudia C, Brunoud
1062 G, Vernoux T, Dumas R, Parcy F. 2017. Structure of the Arabidopsis TOPLESS
1063 corepressor provides insight into the evolution of transcriptional repression. *Proc Natl*
1064 *Acad Sci U S A*. doi:10.1073/pnas.1703054114
1065 Matsumura H, Kusaka N, Nakamura T, Tanaka N, Sagegami K, Uegaki K, Inoue T, Mukai Y.
1066 2012. Crystal structure of the N-terminal domain of the yeast general corepressor Tup1p
1067 and its functional implications. *J Biol Chem* **287**:26528–26538.
1068 doi:10.1074/jbc.M112.369652
1069 McIsaac RS, Oakes BL, Wang X, Dummit KA, Botstein D, Noyes MB. 2013. Synthetic gene
1070 expression perturbation systems with rapid, tunable, single-gene specificity in yeast.
1071 *Nucleic Acids Res* **41**:e57. doi:10.1093/nar/gks1313
1072 Mitchell LA, Chuang J, Agmon N, Khunsriraksakul C, Phillips NA, Cai Y, Truong DM,
1073 Veerakumar A, Wang Y, Mayorga M, Blomquist P, Sadda P, Trueheart J, Boeke JD.
1074 2015. Versatile genetic assembly system (VEGAS) to assemble pathways for expression
1075 in S. cerevisiae. *Nucleic Acids Res* **43**:6620–6630. doi:10.1093/nar/gkv466
1076 Mottis A, Mouchiroud L, Auwerx J. 2013. Emerging roles of the corepressors NCoR1 and SMRT
1077 in homeostasis. *Genes Dev* **27**:819–835. doi:10.1101/gad.214023.113
1078 Nozawa K, Schneider TR, Cramer P. 2017. Core Mediator structure at 3.4 Å extends model of
1079 transcription initiation complex. *Nature* **545**:248–251. doi:10.1038/nature22328
1080 Oberoi J, Fairall L, Watson PJ, Yang J-C, Czimmerer Z, Kampmann T, Goult BT, Greenwood
1081 JA, Gooch JT, Kallenberger BC, Nagy L, Neuhaus D, Schwabe JWR. 2011. Structural
1082 basis for the assembly of the SMRT/NCoR core transcriptional repression machinery.
1083 *Nat Struct Mol Biol* **18**:177–184. doi:10.1038/nsmb.1983
1084 Papamichos-Chronakis M, Conlan RS, Gounalaki N, Copf T, Tzamarias D. 2000. Hrs1/Med3 is
1085 a Cyc8-Tup1 corepressor target in the RNA polymerase II holoenzyme. *J Biol Chem*
1086 **275**:8397–8403. doi:10.1074/jbc.275.12.8397
1087 Perissi V, Jepsen K, Glass CK, Rosenfeld MG. 2010. Deconstructing repression: evolving
1088 models of co-repressor action. *Nat Rev Genet* **11**:109–123. doi:10.1038/nrg2736
1089 Petrenko N, Jin Y, Wong KH, Struhl K. 2017. Evidence that Mediator is essential for Pol II
1090 transcription, but is not a required component of the preinitiation complex in vivo. *eLife*
1091 **6**:e28447. doi:10.7554/eLife.28447
1092 Pierre-Jerome E, Jang SS, Havens KA, Nemhauser JL, Klavins E. 2014. Recapitulation of the
1093 forward nuclear auxin response pathway in yeast. *Proc Natl Acad Sci U S A* **111**:9407–
1094 9412. doi:10.1073/pnas.1324147111
1095 Pierre-Jerome E, Wright RC, Nemhauser JL. 2017. Characterizing Auxin Response Circuits in
1096 Saccharomyces cerevisiae by Flow Cytometry. *Methods Mol Biol Clifton NJ* **1497**:271–
1097 281. doi:10.1007/978-1-4939-6469-7_22
1098 Raya-González J, Oropeza-Aburto A, López-Bucio JS, Guevara-García ÁA, de Veylder L,
1099 López-Bucio J, Herrera-Estrella L. 2018. MEDIATOR18 influences Arabidopsis root

architecture, represses auxin signaling and is a critical factor for cell viability in root meristems. *Plant J Cell Mol Biol* **96**:895–909. doi:10.1111/tpj.14114

Raya-González J, Ortiz-Castro R, Ruíz-Herrera LF, Kazan K, López-Bucio J. 2014. PHYTOCHROME AND FLOWERING TIME1/MEDIATOR25 Regulates Lateral Root Formation via Auxin Signaling in Arabidopsis. *Plant Physiol* **165**:880–894. doi:10.1104/pp.114.239806

Roeder RG. 1996. The role of general initiation factors in transcription by RNA polymerase II. *Trends Biochem Sci* **21**:327–335.

Samanta S, Thakur JK. 2015. Importance of Mediator complex in the regulation and integration of diverse signaling pathways in plants. *Front Plant Sci* **6**:757. doi:10.3389/fpls.2015.00757

Sato S, Tomomori-Sato C, Tsai K-L, Yu X, Sardiu M, Saraf A, Washburn MP, Florens L, Asturias FJ, Conaway RC, Conaway JW. 2016. Role for the MED21-MED7 Hinge in Assembly of the Mediator-RNA Polymerase II Holoenzyme. *J Biol Chem* **291**:26886–26898. doi:10.1074/jbc.M116.756098

Schilbach S, Hantsche M, Tegunov D, Dienemann C, Wigge C, Urlaub H, Cramer P. 2017. Structures of transcription pre-initiation complex with TFIIH and Mediator. *Nature* **551**:204–209. doi:10.1038/nature24282

Schreiber-Agus N, Chin L, Chen K, Torres R, Rao G, Guida P, Skoultchi AI, DePinho RA. 1995. An amino-terminal domain of Mxi1 mediates anti-Myc oncogenic activity and interacts with a homolog of the yeast transcriptional repressor SIN3. *Cell* **80**:777–786.

Siligato R, Wang X, Yadav SR, Lehesranta S, Ma G, Ursache R, Sevilem I, Zhang J, Gorte M, Prasad K, Wrzaczek M, Heidstra R, Murphy A, Scheres B, Mähönen AP. 2016. MultiSite Gateway-Compatible Cell Type-Specific Gene-Inducible System for Plants. *Plant Physiol* **170**:627–641. doi:10.1104/pp.15.01246

Song YH, Estrada DA, Johnson RS, Kim SK, Lee SY, MacCoss MJ, Imaizumi T. 2014. Distinct roles of FKF1, GIGANTEA, and ZEITLUPE proteins in the regulation of CONSTANS stability in Arabidopsis photoperiodic flowering. *Proc Natl Acad Sci* **111**:17672–17677. doi:10.1073/pnas.1415375111

Trumbly RJ. 1992. Glucose repression in the yeast Saccharomyces cerevisiae. *Mol Microbiol* **6**:15–21. doi:10.1111/j.1365-2958.1992.tb00832.x

Tzamarias D, Struhl K. 1994. Functional dissection of the yeast Cyc8-Tup1 transcriptional co-repressor complex. *Nature* **369**:758–761. doi:10.1038/369758a0

Ulmasov T, Hagen G, Guilfoyle TJ. 1997. ARF1, a transcription factor that binds to auxin response elements. *Science* **276**:1865–1868. doi:10.1126/science.276.5320.1865

Wang Z-P, Xing H-L, Dong L, Zhang H-Y, Han C-Y, Wang X-C, Chen Q-J. 2015. Egg cell-specific promoter-controlled CRISPR/Cas9 efficiently generates homozygous mutants for multiple target genes in Arabidopsis in a single generation. *Genome Biol* **16**:144. doi:10.1186/s13059-015-0715-0

Weber E, Engler C, Gruetzner R, Werner S, Marillonnet S. 2011. A Modular Cloning System for Standardized Assembly of Multigene Constructs. *PLOS ONE* **6**:e16765. doi:10.1371/journal.pone.0016765

Wong KH, Struhl K. 2011. The Cyc8-Tup1 complex inhibits transcription primarily by masking the activation domain of the recruiting protein. *Genes Dev* **25**:2525–2539. doi:10.1101/gad.179275.111

Wong MM, Guo C, Zhang J. 2014. Nuclear receptor corepressor complexes in cancer: mechanism, function and regulation. *Am J Clin Exp Urol* **2**:169–187.

Wright RC, Bolten N, Pierre-Jerome E. 2019. flowTime: Annotation and analysis of biological dynamical systems using flow cytometry. Bioconductor version: Release (3.10). doi:10.18129/B9.bioc.flowTime

1150 Yang Y, Li R, Qi M. 2000. In vivo analysis of plant promoters and transcription factors by
1151 agroinfiltration of tobacco leaves. *Plant J* **22**:543–551. doi:10.1046/j.1365-
1152 313x.2000.00760.x
1153 Zhang Y, Gao S, Wang Z. 2010. Structural and functional analysis of amino-terminal enhancer
1154 of split in androgen-receptor-driven transcription. *Biochem J* **427**:499–511.
1155 doi:10.1042/BJ20091631
1156 Zhang Z, Reese JC. 2004. Redundant Mechanisms Are Used by Ssn6-Tup1 in Repressing
1157 Chromosomal Gene Transcription in Saccharomyces cerevisiae. *J Biol Chem*
1158 **279**:39240–39250. doi:10.1074/jbc.M407159200
1159 Zhu J, Jeong JC, Zhu Y, Sokolchik I, Miyazaki S, Zhu J-K, Hasegawa PM, Bohnert HJ, Shi H,
1160 Yun D-J, Bressan RA. 2008. Involvement of Arabidopsis HOS15 in histone deacetylation
1161 and cold tolerance. *Proc Natl Acad Sci* **105**:4945–4950. doi:10.1073/pnas.0801029105
1162
1163
1164
1165

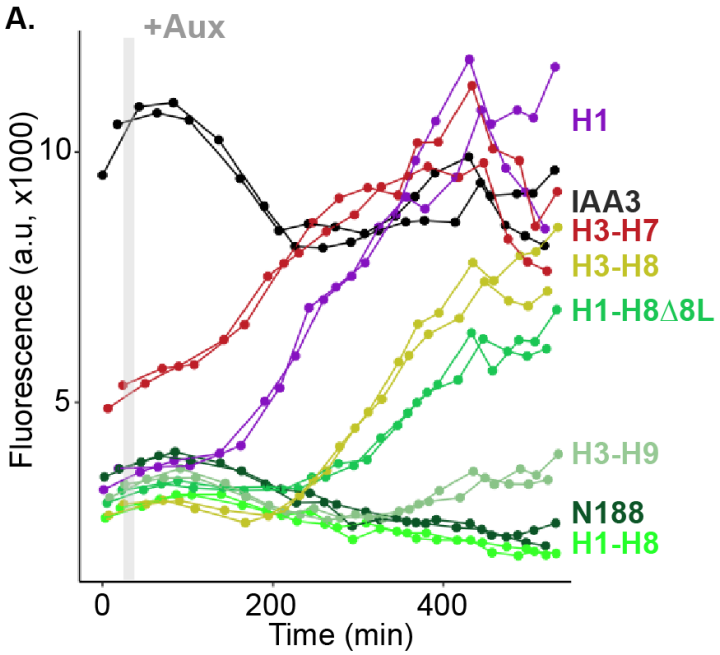

Figure 1 – Figure Supplement 1. Helix 1 and the CRA domain (Helix 3-Helix 8) can act independently to repress transcription. Each color represents two independent time course flow cytometry experiments of the TPL helices indicated, all fused to IAA3 or IAA3 alone (black line). Every point represents the average fluorescence of 5-10,000 individually measured yeast cells (a.u. - arbitrary units). Auxin (IAA-10μM) was added at the indicated time (gray bar, + Aux).

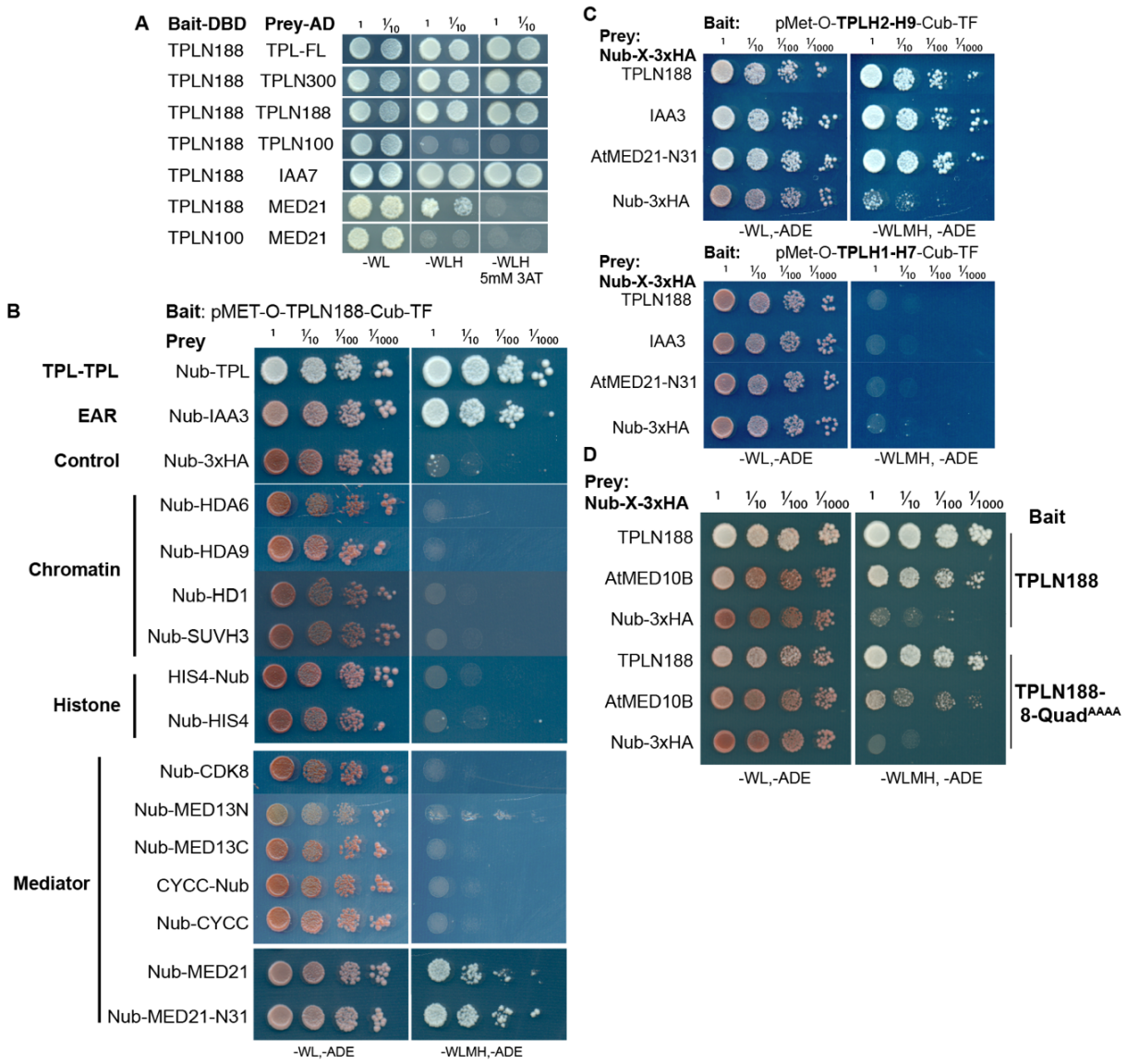

Figure 2 – Figure Supplement 1. The TPL-N terminal domain (TPLN188) interacts with the N-terminus of AtMED21. **A.** Identifying TPL-N terminal domain interactor proteins through Yeast Two Hybrid screening identifies TPL as a problematic Bait protein, as it may silence the activation despite successful binding of a prey protein (see second row from bottom where N188 and MED21 show very weak reporter activity on 3AT). 3AT - 3-Amino-1,2,4-triazole. Plates were measured after 3 days to allow TPL-MED21 interactions to grow. **B.** Identifying TPL-N terminal domain interactor proteins through cytoplasmic split ubiquitin protein interaction assay. We tested the N-terminal and C-terminal portions of MED13 separately and divided the coding sequence at amino acid 967 (MED13N = aa1-967, MED13C = aa968-1908). Each bait tested is the *Arabidopsis* homolog cloned from cDNA from the Col-0 accession, with the

1185 exception of *AtMED13*, which was synthesized *de novo* via Twist
1186 (https://www.twistbioscience.com/). Plates were scanned at 3 days after plating to allow weaker
1187 interactions to develop if they were present. **C.** TPL interacts with MED21 through an interaction
1188 within Helices 8-9. Plates were scanned at 2 days after plating. **D.** The Helix 8 Quadruple
1189 mutation (V145A, E146A, K148A, K149A) does not affect AtMED10B binding to TPL. Plates
1190 were scanned at 3 days after plating. **B-D.** The relative position of the N-terminal portion of
1191 ubiquitin (Nub) is indicated for each bait protein.

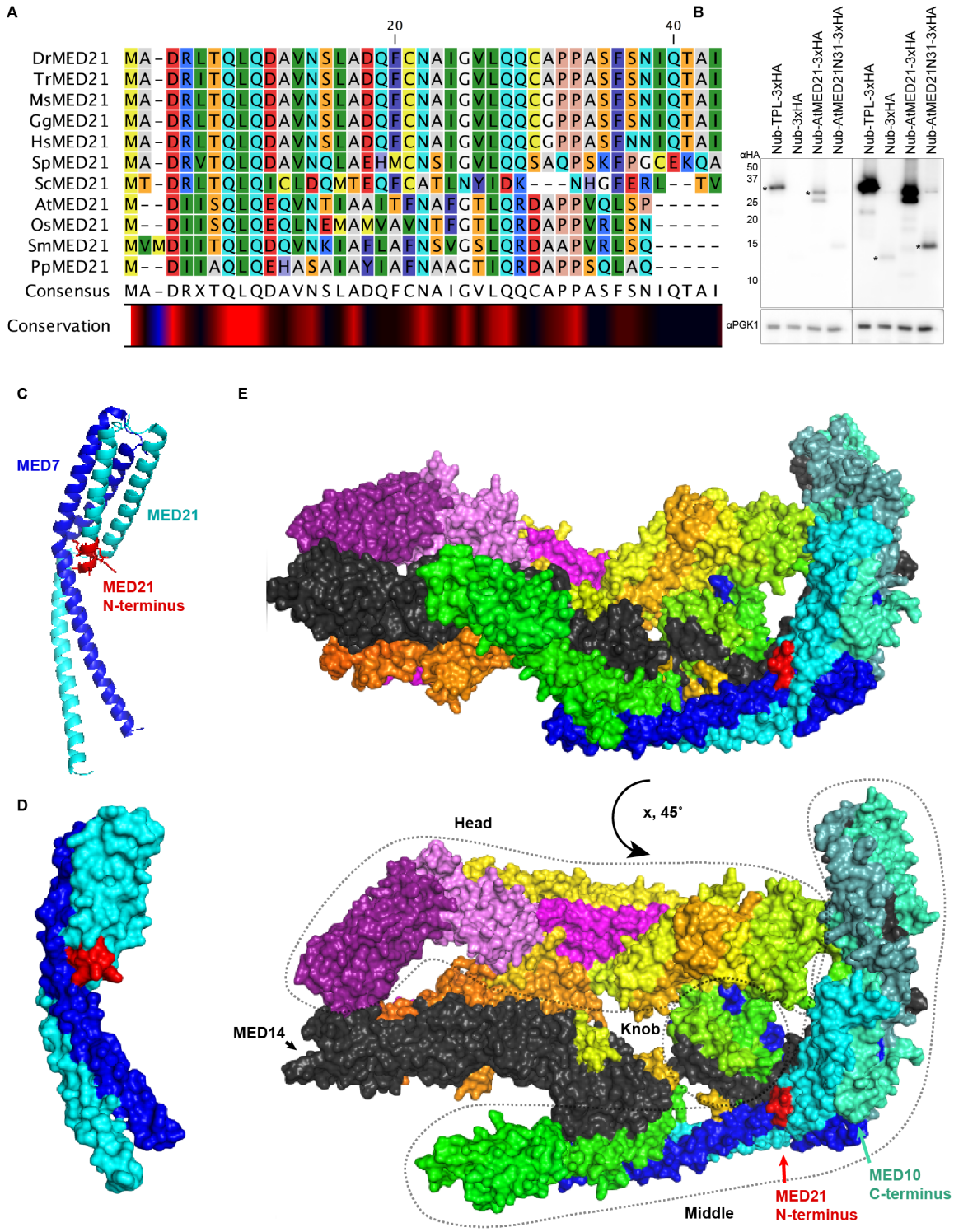

Figure 2 – Figure Supplement 2. Homology and structure of the MED21 subunit of the mediator complex. A. Protein levels of AtMED21 cytoSUS constructs in yeast. Two different exposure times are shown to demonstrate the lower abundance of the truncation with only the

first 31 amino acids of the AtMED21 (N31). Asterisks indicate the size predicted for the indicated protein. **B.** Protein alignment of selected MED21 homologs from various species. Dr - *Drosophila melanogaster*, Tr - *Takifugu rubripes*, Ms - *Mus musculus*, Gg - *Gallus gallus*, Hs - *Homo sapiens*, Sp - *Strongylocentrotus purpuratus*, Sc - *Saccharomyces cerevisiae*, At - *Arabidopsis thaliana*, Os - *Oryza sativa*, Sm - *Selaginella moellendorffii*, Pp - *Physcomitrella patens*. Alignment was performed in CLC sequence viewer 7, using a neighbor joining method. **C-D.** Structure of the MED21 (Cyan) & MED7 (Blue) hetero dimer, adapted from 1YKH, (Baumli et al., 2005). The amino acids in the N-terminus that were solved are highlighted in red up to the 7th amino acid of the yeast MED21. **C.** The cartoon visualization, **D.** Surface visualization. **E.** Core mediator (5N9J, (Nozawa et al., 2017)) with the location of MED21 and MED7 indicated with the same colors from (C-D). In this structure the location of the MED21 N-terminus is again indicated in red, demonstrating its close proximity to the Knob region (dotted circle).

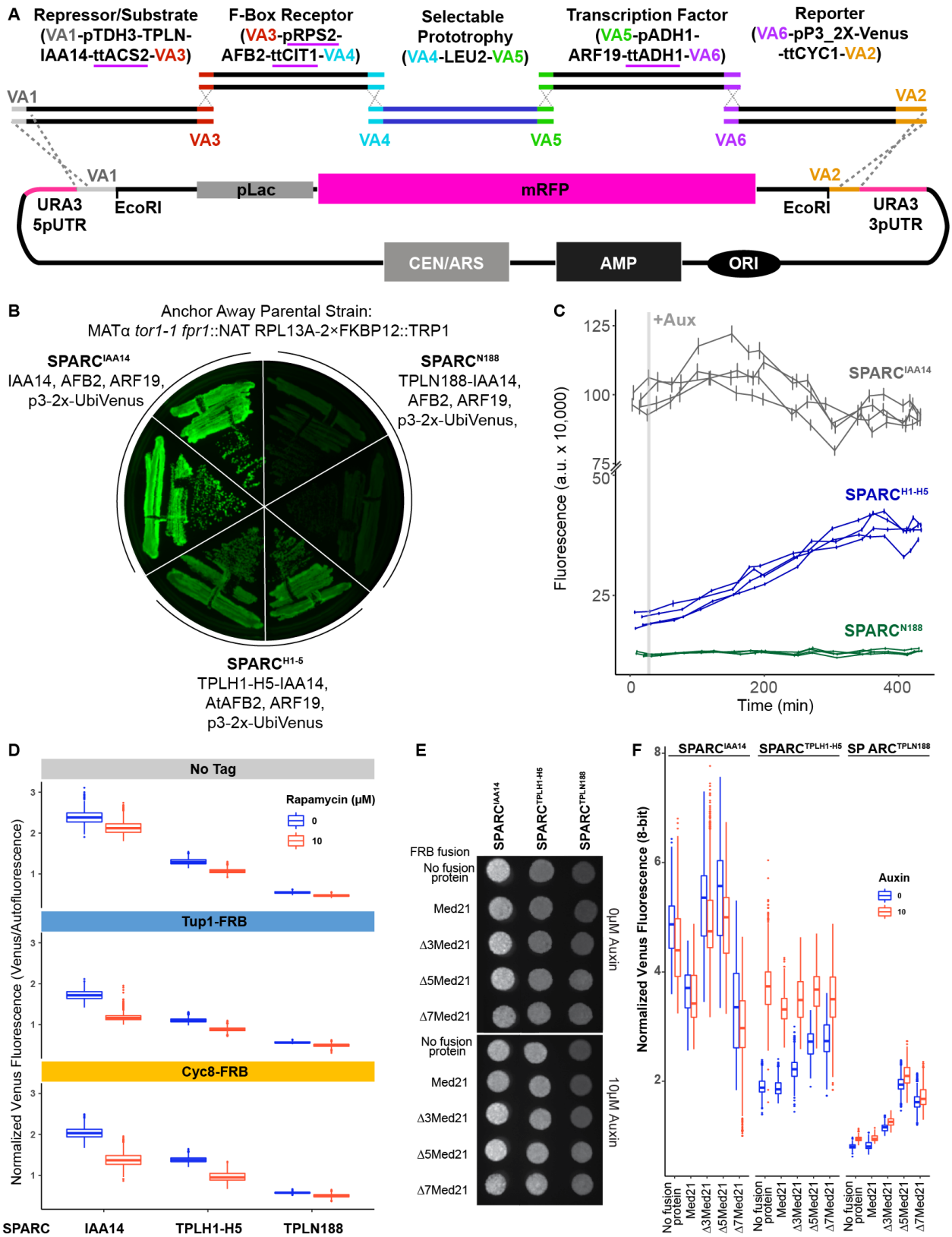
A
Repressor/Substrate (VA1-pTDH3-TPLN-IAA14-ttACS2-VA3)
F-Box Receptor (VA3-pRPS2-AFB2-ttCIT1-VA4)
Selectable Prototrophy (VA4-LEU2-VA5)
Transcription Factor (VA5-pADH1-ARF19-ttADH1-VA6)
Reporter (VA6-pP3_2X-Venus -ttCYC1-VA2)
VA1
VA3
VA4
VA5
VA6
VA2
URA3 5pUTR
EcoRI
pLac
mRFP
URA3 3pUTR
CEN/ARS
AMP
ORI
B
Anchor Away Parental Strain:
MATα tor1-1 fpr1::NAT RPL13A-2×FKBP12::TRP1
SPARCIAA14
IAA14, AFB2, ARF19, p3-2x-UbiVenus
SPARCN188
TPLN188-IAA14, AFB2, ARF19, p3-2x-UbiVenus,
SPARCH1-5
TPLH1-H5-IAA14, AtAFB2, ARF19, p3-2x-UbiVenus
C
+Aux
SPARCIAA14
SPARCH1-H5
SPARCN188
Fluorescence (a.u. x 10,000)
Time (min)
D
No Tag
Tup1-FRB
Cyc8-FRB
Rapamycin (μM)
Normalized Venus Fluorescence (Venus/Autofluorescence)
SPARC
IAA14
TPLH1-H5
TPLN188
E
FRB fusion
No fusion protein
Med21
Δ3Med21
Δ5Med21
Δ7Med21
0μM Auxin
10μM Auxin
F
SPARCIAA14
SPARCTPLH1-H5
SP ARCTPLN188
Normalized Venus Fluorescence (8-bit)
Auxin

1209

1210 **Figure 4 – Figure Supplement 1. Construction and characterization of the Single Locus**
1211 **Auxin Response Circuit (SPARC). A.** Design schematic of the approach utilized to create the
1212 SPARC through a VEGAS assembly approach. Each individual transcriptional unit (TU) was
1213 checked to replace promoters or terminators that utilized identical sequences and replaced with
1214 an alternative sequence indicated by a purple underline. These TUs were assembled into level
1215 1 plasmids by Golden Gate reaction. Subsequently, they were amplified by PCR using primers
1216 specific for the Vegas Adaptor (VA) sequences specific for their TU cassette. In example, for the
1217 first Repressor/Substrate TU the TU was amplified using primers for VA1 and VA3 and purified
1218 by a PCR cleanup column (NEB). The acceptor plasmid was cut with EcoRI and both TU and
1219 acceptor plasmid was transformed into yeast and recombinant plasmids were selected on
1220 synthetic drop out (SDO) plates lacking Leucine. **B.** Primary SPARC transformants were struck
1221 out onto fresh SDO -Leu and imaged for Venus expression, demonstrating varying levels of
1222 reporter expression that correlate with TPL repressor domains. Plasmid DNA was purified from
1223 these strains and sequenced to confirm the proper recombination of TU cassettes. **C.** Time
1224 course flow cytometry of SPARC strains following auxin addition. For all cytometry experiments,
1225 the indicated TPL construct is fused to IAA14, because this IAA works better in haploid yeast
1226 strains that IAA3. Every point represents the average fluorescence of 5-10,000 individually
1227 measured yeast cells (a.u. - arbitrary units). Auxin (IAA-10μM) was added at the indicated time
1228 (gray bar, + Aux). Four independent experiments are shown for each construct. **D.** The yeast
1229 TPL homolog Tup1 and its partner protein Cyc8 do not repress the SPARC. Quantified
1230 fluorescence from the single locus auxin response circuit (SPARC) introduced into Tup1 and
1231 Cyc8 anchor away lines demonstrates no increased fluorescence from the reporter upon
1232 depletion of Tup1 or Cyc8 from the nucleus. Anchor away depletion of Tup1 or Cyc8 results in
1233 slower yeast growth. To normalize for this disparity in growth, Venus fluorescence was
1234 normalized to red autofluorescence, where each pixel was normalized to the corresponding red
1235 autofluorescence collected for that position and plotted as a boxplot. Two individual biological
1236 replicates (two separate experiments) were evaluated, and the data was pooled. **E-F.** Med21 N
1237 terminal deletions are viable in *Saccharomyces* and demonstrate altered SPARC transcriptional
1238 states. **E.** A representative grayscale image of fellow fluorescence of spot plates of yeast strains
1239 carrying SPARC plasmids in Med21 N-terminal deletions. Each is plated at an OD600 of 0.1 on
1240 SDO with or without auxin (10μM IAA). **F.** Venus fluorescence from (**E**) was normalized to red
1241 background (autofluorescence), where each pixel was normalized to the corresponding red

1242 autofluorescence collected for that position and plotted as a boxplot. Two individual biological
1243 replicates (two separate experiments) were evaluated, and the data was pooled and is
1244 presented as boxplots.
1245

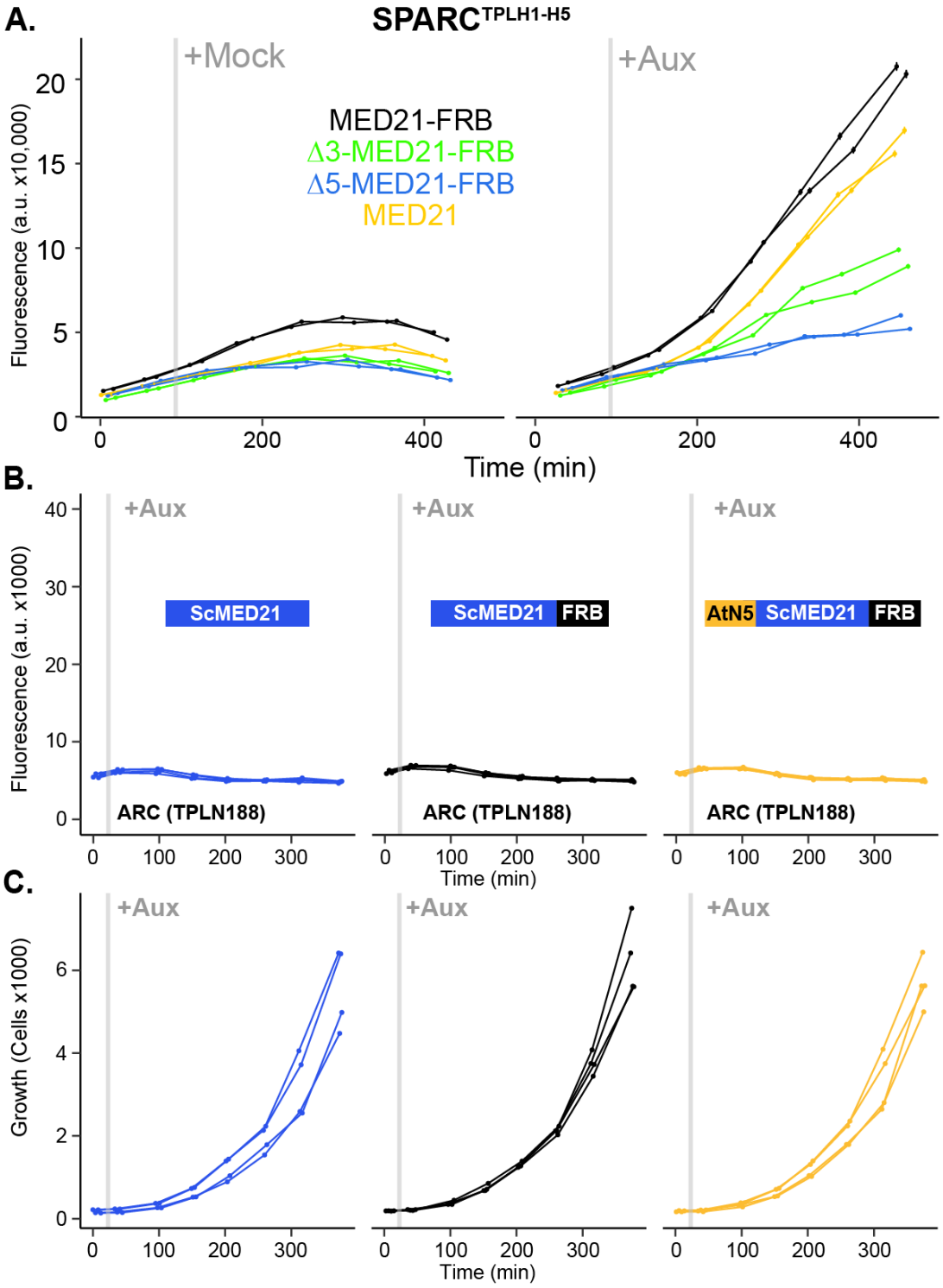

1246

1247 **Figure 4 – Figure Supplement 2. N-terminal ScMed21 deletions impair auxin responsive**
1248 **transcriptional activation A.** Time-course flow cytometry analysis of SPARC^{H1-H5} in wild type
1249 and n-terminal ScMed21 deletions with and without auxin. Genotypes are indicated in the
1250 colored key inset into the graph. Auxin (IAA-10μM) was added at the indicated time (gray bar, +

1251 Aux). **B**. Conversion of the first five amino acids of ScMed21 to the corresponding sequence
1252 from AtMED21 results in an identical repression profile. Time course flow cytometry of SPARC
1253 strains following auxin addition. For all cytometry experiments, the indicated TPL construct is
1254 fused to IAA14, because this IAA performs better in haploid yeast strains that IAA3. Every point
1255 represents the average fluorescence of 5-10,000 individually measured yeast cells (a.u. -
1256 arbitrary units). Auxin (IAA-10μM) was added at the indicated time (gray bar, + Aux). Two
1257 independent experiments are shown for each construct. **C.** Cell growth of the strains in (**B**)
1258 indicate the swap of the N-terminal region had no effect on yeast growth or viability. Data
1259 presented is events per microliter over the time-course of the cytometry experiments.

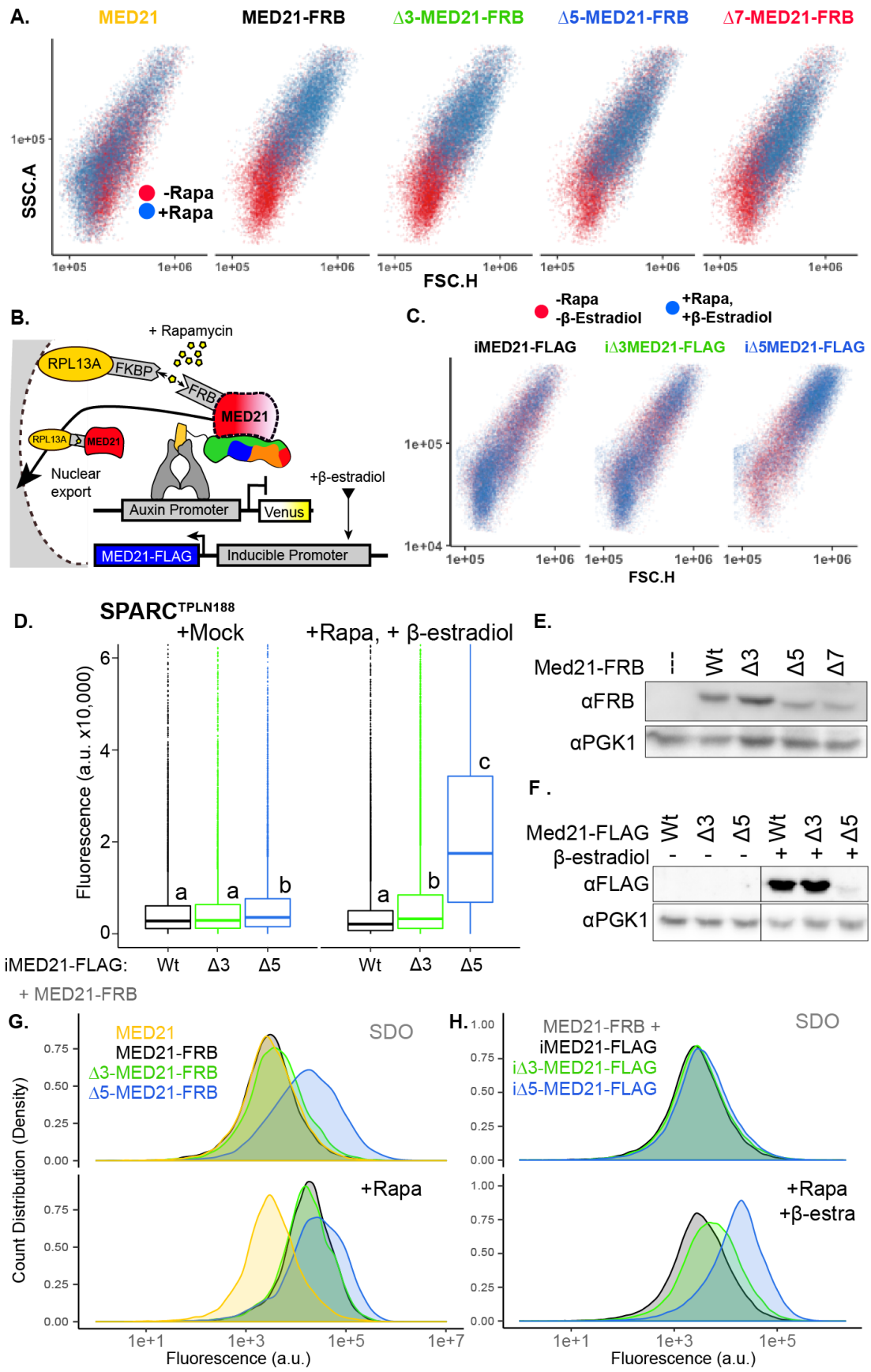
A.
MED21
MED21-FRB
Δ3-MED21-FRB
Δ5-MED21-FRB
Δ7-MED21-FRB
SSC.A
FSC.H
-Rapa
+Rapa
B.
+ Rapamycin
RPL13A
FKBP
FRB
MED21
Nuclear export
+β-estradiol
Auxin Promoter
Venus
MED21-FLAG
Inducible Promoter
C.
-Rapa -β-Estradiol
+Rapa, +β-Estradiol
iMED21-FLAG
iΔ3MED21-FLAG
iΔ5MED21-FLAG
FSC.H
D.
SPARC TPLN188
+Mock
+Rapa, + β-estradiol
Fluorescence (a.u. x10,000)
iMED21-FLAG: Wt Δ3 Δ5 Wt Δ3 Δ5
+ MED21-FRB
E.
Med21-FRB
αFRB
αPGK1
F .
Med21-FLAG
β-estradiol
αFLAG
αPGK1
G.
MED21
MED21-FRB
Δ3-MED21-FRB
Δ5-MED21-FRB
SDO
+Rapa
Count Distribution (Density)
Fluorescence (a.u.)
H.
MED21-FRB +
iMED21-FLAG
iΔ3-MED21-FLAG
iΔ5-MED21-FLAG
SDO
+Rapa
+β-estra
Fluorescence (a.u.)

1260

1261 **Figure 4 – Figure Supplement 3. Inducible MED21 rescues rapamycin induced yeast**
1262 **growth defects. A.** Depletion of nuclear ScMed21 by Rapamycin increased cell size even in
1263 short time-courses, consistent with its essential role in many core pathways. Scatterplots of side
1264 scatter area by forward scatter height (SSC.A x FSC.H) indicate large scale increases in cell
1265 size in populations of yeast with (blue) or without (red) Rapamycin treatment. **B.** Schematic of
1266 AtARCSc combined with methods for inducible expression and nuclear depletion of MED21. In
1267 Anchor Away, the yeast ribosomal protein 13A (RPL13A) is fused to the rapamycin binding
1268 protein FKBP. Addition of Rapamycin induces dimerization between FKBP and any target
1269 protein fused to FRB, resulting in removal of the target protein from the nucleus. For these
1270 experiments, AtARCSc was assembled into a single plasmid (SPARC) rather than being
1271 integrated into separate genomic loci (Figure 4 – Figure Supplement 1). Estradiol-inducible
1272 ScMed21 (iMed21) made it possible to replace wild-type MED21 with targeted deletions or
1273 mutations. **C.** Inducible Med21 (iMed21) wild type and variants cell size were examined before
1274 (red) and after (blue) treatment with Rapamycin and b-estradiol to simultaneously deplete the
1275 wild-type Med21-FRB fusion, and induce the transcription of the Med21 variant. Scatterplots of
1276 side scatter area by forward scatter height (SSC.A x FSC.H) demonstrate a less disrupted cell
1277 size compared to Anchor Away strains in (**A**). **D.** Rapid replacement of Med21-FRB with
1278 inducible Med21-FLAG demonstrated the requirement for the ScMed21 N-terminus in TPL
1279 repression. iMed21 isoforms were induced by addition of β-estradiol (20μM) for 4 hours followed
1280 by Rapamycin addition. Fluorescence was quantified by cytometry after 300 minutes. Lower
1281 case letters indicate significant difference (ANOVA and Tukey HSD multiple comparison test;
1282 $p<0.001$). **E-F.** Protein abundance of ScMed21 variants was tested by SDS-PAGE & western
1283 blot **E.** Stably integrated Med21-FRB variants. **F.** Induced iMed21-FLAG variants. **G-H.**
1284 Histograms of Venus fluorescence in inducible Med21 (iMed21) strains demonstrate that
1285 populations were evenly distributed around a single mean, suggesting we were observing the
1286 immediate effects of the Med21 deletions. The histograms were built using ggplots Density
1287 function to create a visualization of count distribution. These samples were tested at 300
1288 minutes (as in Figure 4D) and plotted to visualize cells at the equivalent stage of growth, Med21
1289 depletion, and induction.
1290
1291
1292

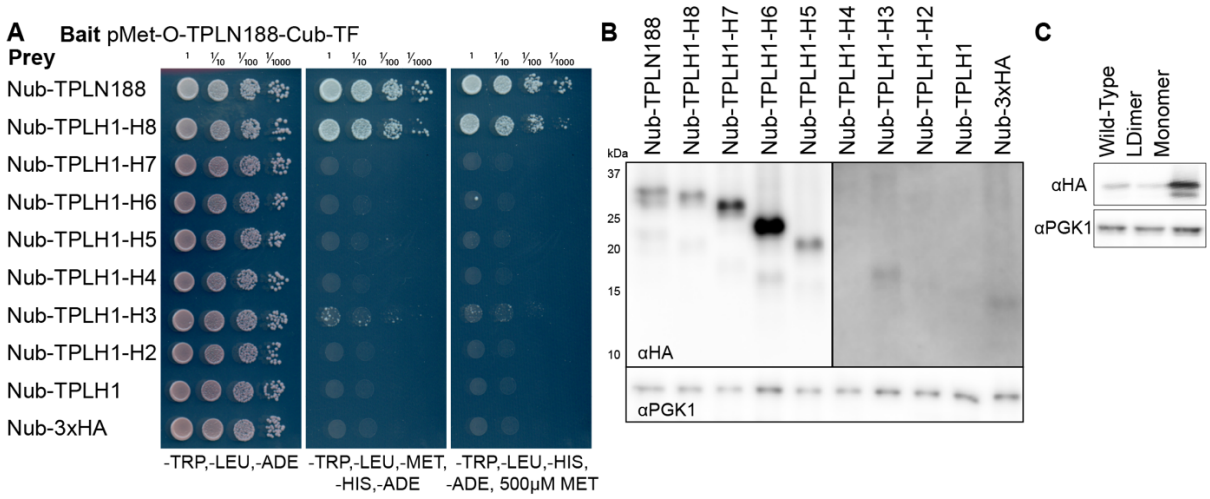

Figure 5 – Figure Supplement 1. TPL multimerization requires Helix 8. A. Cytoplasmic split ubiquitin interaction (cytoSUS) assay on serial deletions of TPL. Interaction of bait and prey proteins reconstitute split ubiquitin, release a synthetic transcription factor that allows growth on media lacking Histidine and Adenine. The expression level of the bait protein can be repressed through increased Methionine in the media. **B**. Protein levels of Nub-TPL fusions were tested by PAGE and western blotting for the c-terminal 3xHA epitope tag included in all constructs. Deletions longer than H1-4 are detectable at higher levels (left panel), whereas shorter isoforms required longer exposure times to detect (right panel). Total protein loading levels were tested by the housekeeping gene PGK1 (bottom panel). **C.** Protein expression analysis by western blotting of tetramerization mutants expressed in yeast for cytoSUS interaction assay in Figure 5I. Prey constructs are C-terminally fused to 2xHA. Total protein loading levels were tested by blotting against the housekeeping gene PGK1 (bottom panel).

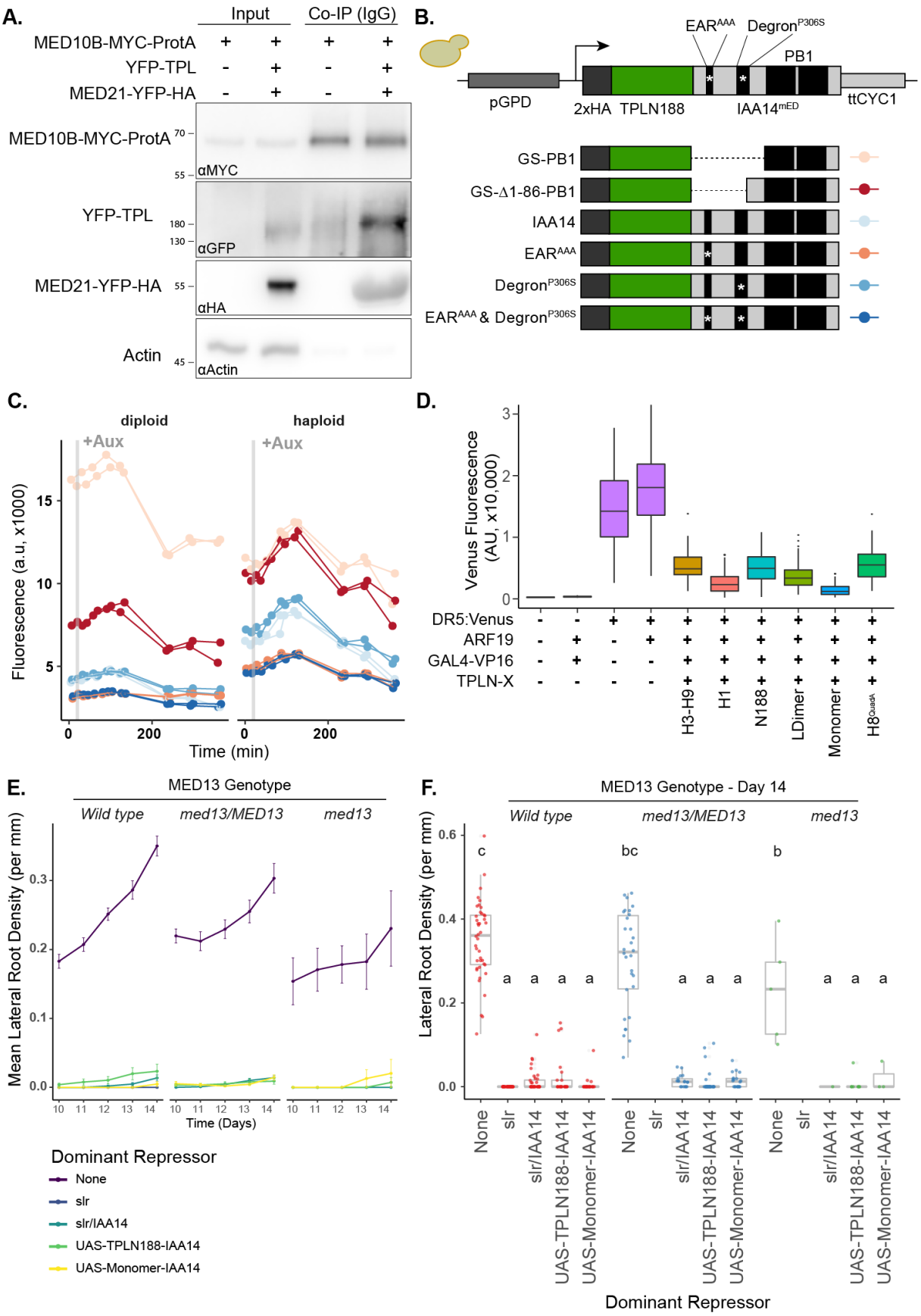
A.
Input
Co-IP (IgG)
MED10B-MYC-ProtA
YFP-TPL
MED21-YFP-HA
αMYC
αGFP
αHA
αActin
B.
EARAAA
DegronP306S
PB1
pGPD
2xHA
TPLN188
IAA14mED
ttCYC1
GS-PB1
GS-Δ1-86-PB1
IAA14
EARAAA
DegronP306S
EARAAA & DegronP306S
C.
diploid
haploid
+Aux
Fluorescence (a.u, x1000)
Time (min)
D.
Venus Fluorescence (AU, x10,000)
DR5:Venus
ARF19
GAL4-VP16
TPLN-X
H3-H9
H1
N188
LDimer
Monomer
H8QuadA
E.
MED13 Genotype
Wild type
med13/MED13
med13
Mean Lateral Root Density (per mm)
Time (Days)
Dominant Repressor
None
slr
slr/IAA14
UAS-TPLN188-IAA14
UAS-Monomer-IAA14
F.
MED13 Genotype - Day 14
Wild type
med13/MED13
med13
Lateral Root Density (per mm)
Dominant Repressor

1308

1309 **Figure 6 – Figure Supplement 1. The TPL-MED21 interaction is required for repression in**
1310 **plants. A.** MED21 and TPL Co-Immunoprecipitated with AtMED10B from tobacco extracts.
1311 Each construct was expressed under the viral 35S promoter, and tissues were harvested after 2
1312 days of injection. MED10B was purified by incubation with IgG sepharose beads (see methods),
1313 and the presence of interacting proteins was determined by western blotting. Actin was used as
1314 a control to determine the efficacy of washing. **B-C.** Engineering and prototyping a variant of
1315 TPLN-IAA14^{mED} which carries mutations in the EAR domain (EAR^{AAA}) and in the degron
1316 (P306S) in yeast. **B.** Cartoon schematic of the mutations tested during prototyping of the
1317 TPLN188-IAA14mED construct. In each case the identical glycine-serine linker (GS) was used
1318 as the flexible linker between the 2xHA-TPLN188 protein and the portion of IAA14 retained in
1319 the construct. **C.** Time course flow cytometry of TPLN-IAA14^{mED} strains following auxin addition.
1320 Strains containing the TPLN-IAA14^{mED} was tested in both haploid and diploid strains and
1321 demonstrated similar repression profiles. Every point represents the average fluorescence of 5-
1322 10,000 individually measured yeast cells (a.u. - arbitrary units). Auxin (IAA-10μM) was added at
1323 the indicated time (gray bar, + Aux). Two independent experiments are shown for each
1324 construct. **D.** Transient expression of indicated TPL constructs in tobacco. DR5:Venus - the
1325 synthetic DR5 auxin promoter (Ulmasov et al., 1997) driving Venus, ARF19 - p35S:AtARF19-
1326 1xFLAG, GAL4:VP16 - pUBQ10:GAL4-VP16, TPLN-X-UAS-TPL-IAA14^{mED} with various TPL
1327 truncations or mutations. **E-F.** The TPL-N terminus functions as a repressor independently of
1328 the MED13 component of the Mediator CDK8 Kinase module in *Arabidopsis*. The dominant
1329 lateral root repression constructs (UAS-TPLN188-IAA14, UAS-Monomer-IAA14) and the
1330 dominant *slr* mutant were crossed to the *med13* mutant (*gct-5*, a.k.a. *mab2-2*, *SAIL_1169H11*).
1331 We performed time-course lateral root density assays and genotyped the progeny in the F1 and
1332 F2 generations. We observed a ~1% transmission rate of *gct-5* homozygotes. **E.** Time-course of
1333 the mean of lateral root density over days 10-14 post germination plus and minus standard
1334 error. **F.** Boxplots of lateral root density for day 14 (**E.**). Lower case letters indicate significant
1335 difference (ANOVA and Tukey HSD multiple comparison test; $p<0.001$).
1336
1337

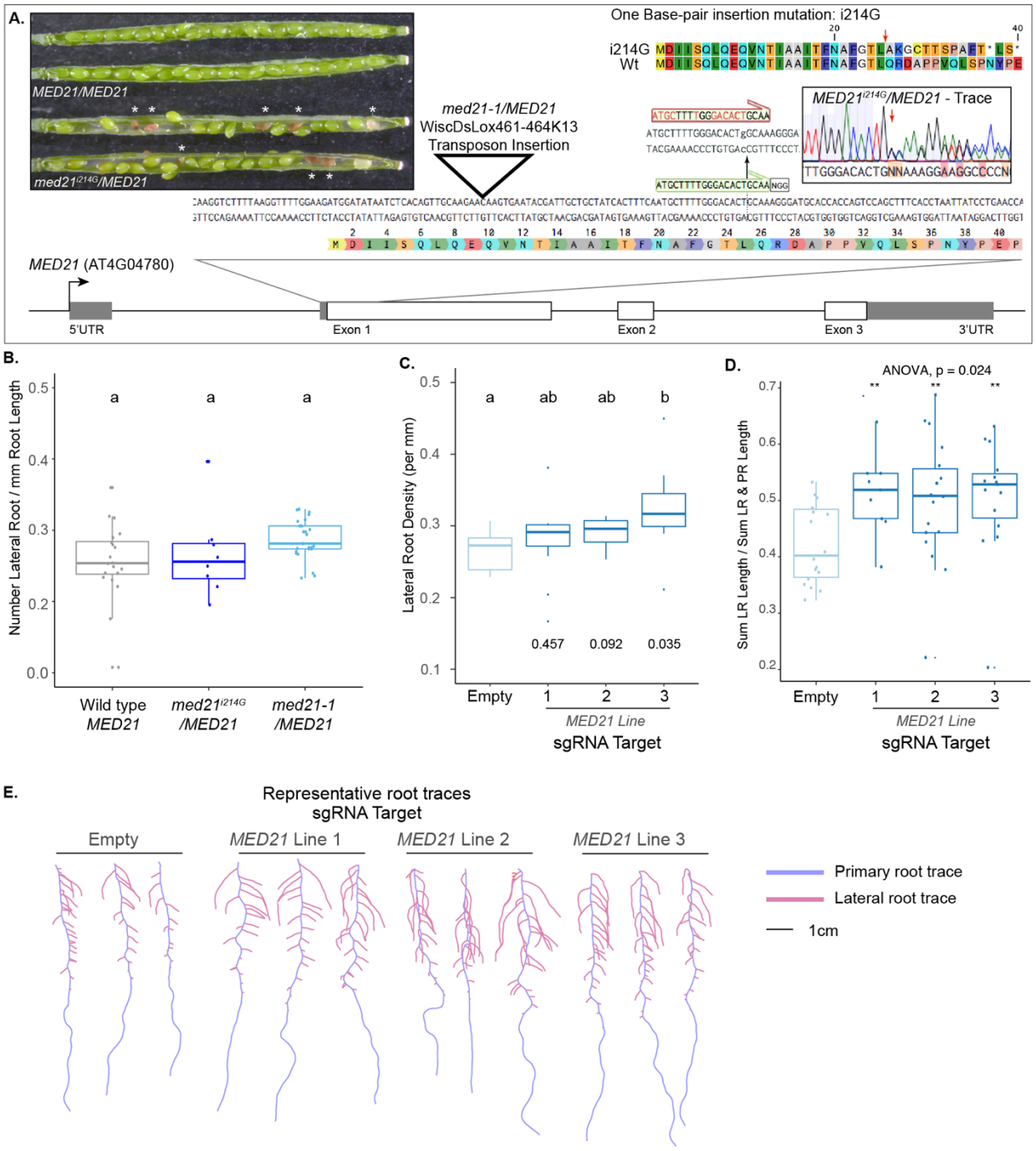

Figure 6 – Figure Supplement 2. The essential gene MED21 is required for normal lateral root development in plants. A. Identification and characterization of a novel CAS9-based insertional mutation in *MED21*. The *MED21* genomic locus (AT4G04780) is shown as a cartoon, with a zoom in on the beginning of the coding sequence highlighted with the amino acid sequence. The location of the *med21/MED21* mutant (WiscDsLox461-464K13, see triangle), and the sgRNA we employed (see green annotation and NGG PAM site) highlighted. The

1345 insertion of a G at nucleotide position +214 after the transcriptional start site abrogates the
1346 sgRNA site (red annotation above with i214G). A representative sequencing trace demonstrates
1347 the position where the heterozygote carries i215G, and the predicted effect to the coding
1348 sequence is shown at the top right – a red arrow indicates the first codon affected by the i214G
1349 mutation. The Inset pictures at the top left demonstrate the embryo lethality phenotype in
1350 *med21*^{i214G}*/MED21* heterozygote siliques. White asterisks indicate the embryos that have begun
1351 to degenerate. These aborted seeds are visibly brown indicating that fertilization took place
1352 allowing the seed coat to form before development failed. **B.** *med21*/*MED21* heterozygotes are
1353 haplo-sufficient for lateral root development. Lateral root density (number of lateral roots /
1354 primary root length) was calculated at 10 days post germination. Lower case letters indicate
1355 significant difference (ANOVA and Tukey HSD multiple comparison test; $p<0.005$). **C.** MED21-
1356 CAS9 repressors targeted to MED21 display increased lateral root densities. Lateral root
1357 density (number of lateral roots / primary root length) was calculated at 10 days post
1358 germination. Numbers below boxplots are p-values for pairwise comparisons with control using
1359 a Wilcoxon rank sum test. **D.** Ratio of lateral root lengths to total root lengths (lateral root
1360 lengths + primary root length) in dCAS9 repressor lines targeting *MED21* calculated at 10 days
1361 post germination. Statistical tests (ANOVA and Wilcox test) are reported above the graph. **G.**
1362 Representative root traces of dCAS9 repressor lines targeting *MED21* calculated at 10 days
1363 post germination.
1364